

Identifying climate impacts from different Stratospheric Aerosol Injection strategies in UKESM1

Alice F. Wells^{1*}, Matthew Henry¹, Ewa M. Bednarz^{2,3,4}, Douglas G.
MacMartin⁴, Andy Jones⁵, Mohit Dalvi⁵ and James M. Haywood^{1,5}

¹Faculty of Environment, Science and Economy, Department of Mathematics and Statistics, University of
Exeter, Exeter, EX4 4QE, United Kingdom

²Cooperative Institute for Research in Environmental Sciences (CIRES), University of Colorado Boulder,
Boulder, CO, USA

³NOAA Chemical Sciences Laboratory (NOAA CSL), Boulder, CO, USA

⁴Sibley School of Mechanical and Aerospace Engineering, Cornell University, Ithaca, NY, USA

⁵Met Office, Exeter, EX1 3PB, United Kingdom

Key Points:

- We compare the climate impacts of equatorial and multi-latitude Stratospheric Aerosol injection strategies under the GeoMIP G6 framework
- We demonstrate that an off-equatorial multi-latitude injection strategy minimises unfavourable climate impacts
- This research highlights the importance of injection location in determining the impacts of SAI on the climate

*Current address, Faculty of Environment, Science and Economy, Department of Mathematics and Statistics, University of Exeter, Exeter, EX4 4QE, United Kingdom

Corresponding author: Alice F Wells, a.wells@exeter.ac.uk

Abstract

Stratospheric Aerosol Injection (SAI) is a proposed method of climate intervention aiming to reduce the impacts of human-induced global warming by reflecting a portion of incoming solar radiation. Many studies have demonstrated that SAI would successfully reduce global-mean surface air temperatures, however the vast array of potential scenarios and strategies for deployment result in a diverse range of climate impacts. Here we compare two SAI strategies - a quasi-equatorial injection and a multi-latitude off-equatorial injection - simulated with the UK Earth System Model (UKESM1), both aiming to reduce the global-mean surface temperature from that of a high-end emissions scenario to that of a moderate emissions scenario. Both strategies effectively reduce global mean surface air temperatures by around 3°C by the end of the century; however, there are significant differences in the resulting regional temperature and precipitation patterns. We compare changes in the surface and stratospheric climate under each strategy to determine how the climate response depends on the injection location. In agreement with previous studies, an equatorial injection results in a tropospheric overcooling in the tropics and a residual warming in the polar regions, with substantial changes to stratospheric temperatures, water vapour and circulation. However, we demonstrate that by utilising a feedback controller in an off-equatorial injection strategy, regional surface temperature and precipitation changes relative to the target can be minimised. We conclude that moving the injection away from the equator minimises unfavourable changes to the climate, calling for a new series of inter-model SAI comparisons using an off-equatorial strategy.

Plain Language Summary

Stratospheric Aerosol Injection (SAI) is a method to tackle the impacts of global warming and involves reflecting some of the sun's rays away from Earth. Different strategies for implementing SAI can have various effects on the climate. This study compares two strategies - one injecting at the equator and the other at different latitudes. Both strategies successfully lower global temperatures, but they also lead to different regional climate changes. The equatorial strategy cools the tropics too much and doesn't cool the poles enough. Whereas the off-equatorial strategy minimises some of the negative impacts seen in the equatorial strategy. In summary, injecting aerosols away from the equator avoids unfavourable climate impacts.

1 Introduction

The climate is warming at an unprecedented rate with global mean temperatures projected to reach or exceed the 1.5°C Paris agreement temperature goal within the next 20 years (Masson-Delmotte et al., 2021). Increases in the number of extreme weather events have already been observed in recent years including extreme precipitation events, droughts, and heatwaves. Under global warming, the frequency and intensity of such events are projected to increase (Seneviratne et al., 2021). Mitigation efforts have been made with net-zero pledges reducing projected 2030 global emissions by 7.5% (Programme, 2021), however due to the long lifetime of CO₂ the impacts of climate change are likely to continue. These factors have resulted in an increasing interest in climate intervention strategies.

Solar climate intervention (SCI), otherwise known as solar radiation modification (SRM), methods aim to increase the planetary albedo and induce a surface cooling, thereby reducing some of the undesirable impacts of global warming on the weather and climate. These proposed techniques aim to reduce increasing temperatures whilst mitigation efforts continue and greenhouse gases are removed from the atmosphere. Recently, support for SRM research has grown with two reports advocating for more robust scientific

68 research. The US National Academies of Sciences, Engineering and Medicine (NASEM)
69 report on solar geoengineering research and research governance (NASEM, 2021) pro-
70 posed a \$200 million investment into a research program to better understand the risks,
71 benefits and impacts of SCI strategies. The United Nations Environment Programme
72 (UNEP) also called for robust, equitable and rigorous trans-disciplinary research to re-
73 duce uncertainties associated with SRM (UNEP, 2023).

74 One of the proposed methods of SRM, Stratospheric Aerosol Injection (SAI), origi-
75 nally proposed by Budyko (1977) and revisited by Crutzen (2006), aims to mimic the
76 effect of a large volcanic eruption by injecting SO_2 into the stratosphere to produce a
77 layer of sulfate aerosols which can reflect a small portion of the incoming solar radiation.
78 Whilst there are some differences between a single pulse injection of SO_2 from a volcanic
79 eruption and the continual injection needed to consistently cool the planet (MacMartin
80 et al., 2016; Robock et al., 2013), volcanic eruptions act as natural analogues for assess-
81 ing the capability of global climate models to model SAI (e.g. (Trenberth & Dai, 2007)).
82 Model uncertainties (Visioni et al., 2021; Visioni, Bednarz, et al., 2023; Bednarz, Visioni,
83 Kravitz, et al., 2023; Henry et al., 2023) and different SAI scenario choices, including the
84 choice of baseline emissions scenario (Fasullo & Richter, 2022), injection location or strat-
85 egy (Kravitz et al., 2019; Bednarz, Butler, et al., 2023; Zhang et al., 2023), temperature
86 target (Hueholt et al., 2023; MacMartin et al., 2022; Visioni, MacMartin, et al., 2023;
87 Bednarz, Visioni, Butler, et al., 2023) and timing of SAI deployment can result in dif-
88 ferent large-scale climate responses and the associated regional impacts.

89 To assess model uncertainties, similar experiments can be compared across differ-
90 ent models. This is a common approach in climate modelling, with the results from mul-
91 tiple models forced by nominally identical shared socio-economic pathway (SSP) green-
92 house gas emission scenarios being frequently used in the climate change context (e.g.
93 (Masson-Delmotte et al., 2021)). Similarly, inconsistent SRM results between multiple
94 models (e.g. (Rasch et al., 2008; A. Jones et al., 2010)) motivated the Geoengineering
95 Model Intercomparison Project (GeoMIP) as a means to help untangle those differences
96 by creating a set of standardised experiments. The latest GeoMIP experiments, which
97 align with the latest CMIP6 scenarios, include G6solar and G6sulfur (Kravitz et al., 2013,
98 2015). The aim of these experiments was to reduce global mean surface air temperatures
99 under the otherwise high-end SSP5-8.5 emissions scenario to those of the more moder-
100 ate SSP2-4.5 (O'Neill et al., 2016). This was achieved by either reducing the solar con-
101 stant (G6solar) or by injecting SO_2 between 10°N and 10°S and between 18 and 20 km
102 (G6sulfur).

103 Outside of GeoMIP, experiments using the Community Earth System Model (CESM)
104 and UKESM1 have been performed using control theory to modify the annual injection
105 of SO_2 across multiple locations (MacMartin & Kravitz, 2019). Studies include the Geo-
106 engineering Large ENSEMBLE project (GLENS; Tilmes, Richter, Kravitz, et al. (2018))
107 and the Assessing Responses and Impacts of Solar climate intervention of the Earth sys-
108 tem with Stratospheric Aerosol Injection project (ARISE-SAI; Richter et al. (2022)). These
109 experiments injected SO_2 at multiple latitudes (30°S , 15°S , 15°N , 30°N) away from the
110 equator and controlled not only the global-mean surface air temperature, but also its in-
111 terhemispheric and equator-to-pole temperature gradients (MacMartin et al., 2017; Kravitz
112 et al., 2017). The motivation behind the inclusion of the latter two temperature targets
113 under a feedback controller were to reduce the tropical overcooling and polar undercool-
114 ing simulated under many equatorial injections (Kravitz et al., 2016) whilst also min-
115 imising any changes to the position of the InterTropical Convergence Zone (ITCZ) and
116 the associated precipitation patterns (J. M. Haywood et al., 2013). Under the GLENS
117 SAI scenario framework, Kravitz et al. (2019) demonstrated that using a multi-latitude
118 off-equatorial injection strategy in CESM1 can minimise the residual impacts on regional
119 surface air temperature and precipitation when compared to the same scenario using an
120 equatorial injection strategy. In that case, temperatures were held constant with SAI at

2020 levels under the high-end RCP8.5 warming scenario, requiring large injections of SO₂ by the end of the century.

Here, we pursue a methodology similar to that in Kravitz et al. (2019); we compare the global climate response to a quasi-equatorial injection strategy, G6sulfur, and an equivalent off-equatorial multi-latitude injection strategy, G6controller. G6controller uses the feedback controller (MacMartin et al., 2018; Kravitz et al., 2017; MacMartin & Kravitz, 2019) to meet the yearly global mean surface air temperature of SSP2-4.5 as in the G6sulfur scenario design. It is also designed to meet the interhemispheric and equator-to-pole temperature gradients similar to GLENS and ARISE. By making the comparison between G6sulfur and G6controller we can determine if the results seen in Kravitz et al. (2019), comparing GLENS to an equatorial injection, are consistent with those from UKESM1 and under the GeoMIP framework. After describing the model and the scenario and strategy design in Sect. 2 we compare the injection rate of each strategy and their ability to meet the desired temperature targets (Sect. 3). We then compare the surface air temperature (Sect. 4) and precipitation response (Sect. 5.1) under each strategy before we analyse the stratospheric response in Sect. 6.

2 Methods

Previous studies have documented the GeoMIP G6sulfur simulations and the UKESM1 model (e.g. (A. Jones et al., 2020; J. M. Haywood et al., 2022)), so only a brief summary of the G6sulfur simulations and the model are provided here. Similarly, the implementation of the controller (Kravitz et al., 2017; MacMartin & Kravitz, 2019) within the UKESM1 model is described in Henry et al. (2023).

2.1 Model Description

UKESM1, the latest UK Earth system model, is described by Sellar et al. (2019). It consists of the HadGEM3 coupled physical climate model with a resolution of 1.25° latitude by 1.875° longitude with 85 vertical levels and a model top at approximately 85 km. This is coupled to a 1° resolution ocean model with 75 levels (Storkey et al., 2018). It includes additional interactive components to model tropospheric and stratospheric chemistry (Archibald et al., 2020), ocean biogeochemistry (Yool et al., 2013), sea ice (Ridley et al., 2018), land surface and vegetation (Best et al., 2011) and aerosols (Mann et al., 2010). The merged stratospheric and tropospheric scheme, StratTrop as described by Archibald et al. (2020), simulates interactive chemistry from the surface to the top of the model which includes the oxidation reactions responsible for sulphate aerosol production (Sellar et al., 2019). Evaluation of the evolution of stratospheric aerosols from explosive volcanic eruptions in UKESM1 have been performed and the model shows reasonable fidelity (e.g. (Dhomse et al., 2020; Wells, Jones, Osborne, et al., 2023)).

2.2 Simulation set up/design and analysis framework

This study analyses four sets of simulations from 2020 to 2100. These include two baseline scenarios which follow the Shared Socioeconomic Pathways SSP2-4.5 and SSP5-8.5 (O'Neill et al., 2016), and two stratospheric aerosol injection strategies, G6sulfur and G6controller. As described in Kravitz et al. (2015), the aim of G6sulfur is to modify high-end emission scenario SSP5-8.5 simulations so that the global mean surface air temperature is reduced to that of the moderate emissions scenario SSP2-4.5. In the UKESM1 G6sulfur simulations, the SSP5-8.5 decadal-mean global mean surface air temperature is reduced to within 0.2 K of the corresponding SSP2-4.5 temperature through manually adjusting the magnitude of SO₂ injection into the lower stratosphere (A. Jones et al., 2020). In particular, the injection is applied uniformly between 10°N - 10°S along the

168 Greenwich meridian at 18 - 20 km, with the amount of SO₂ adjusted every 10 years to
 169 meet SSP2-4.5 targets.

170 Whilst G6controller follows the same overarching scenario as G6sulfur, reducing
 171 global mean surface air temperature from SSP5-8.5 to SSP2-4.5, the injection strategy
 172 is more complex. Similarly to the GLENS (Tilmes, Richter, Kravitz, et al., 2018) and
 173 the ARISE-SAI (Richter et al., 2022) strategies, G6controller injects SO₂ at four lati-
 174 tudes - 30°N, 15°N, 15°S and 30°S - and a slightly higher altitude of 21.5 km using a feed-
 175 back algorithm (as described by MacMartin et al. (2018); Kravitz et al. (2017); Henry
 176 et al. (2023)) that adjusts the injection rate at each location to meet simultaneous tem-
 177 perature targets, namely: the global mean surface air temperature (T_0), the interhemi-
 178 spheric surface air temperature gradient (T_1), and the equator-to-pole surface air tem-
 179 perature gradient (T_2). T_1 and T_2 are defined in equation 1 from Kravitz et al. (2017).
 180 One subtle difference between the implementation of the controller in these simulations
 181 and the previous works (e.g. (Tilmes, Richter, Kravitz, et al., 2018; Kravitz et al., 2019;
 182 Richter et al., 2022; Henry et al., 2023)) is that, rather than fixed targets, T_0 , T_1 and
 183 T_2 are transient values determined from the SSP2-4.5 simulations.

184 While many of the results that are presented here show either the global or zonal
 185 mean responses, in Section 4 we also present results of regional surface air temperature
 186 changes by calculating regional means over the 46 land-only reference regions (Iturbide
 187 et al., 2020) produced for the Intergovernmental Panel on Climate Change Assessment
 188 Report 6 (Masson-Delmotte et al., 2021). These areas (henceforth AR6) are shown in
 189 Figure S1 with abbreviations for region names, coloured by continent.

190 3 Large scale temperature targets and SO₂ injections

191 The SO₂ injection rate in both strategies is comparable throughout the 80 years
 192 of the simulations (Fig. 1). Cumulatively G6sulfur injects around 10% more than G6controller
 193 (705 Tg compared to 645 Tg) to reach roughly the same global mean surface temper-
 194 atures (Fig. 2a). The lower efficiency of G6sulfur compared to G6controller is at least
 195 in part driven by the differences in the injection altitudes, 21.5 km for G6controller and
 196 18-20 km for G6sulfur; a lower injection altitude reduces lifetime of sulfate aerosols and,
 197 thus, the overall efficiency. Studies with the CESM model have also shown that equa-
 198 torial injections can be less efficient at offsetting global mean temperatures than off-equatorial
 199 strategies (e.g. (Kravitz et al., 2019; Zhang et al., 2023)). There are also studies which
 200 show a greater efficiency and temperature change from a radiative forcing applied at higher
 201 latitudes relative to one applied at the equator (e.g. (Zhao et al., 2021)) In this case, it
 202 is likely a combination of effects, however the difference in injection altitude is likely the
 203 dominant cause of the difference in efficiency as simulations with a predecessor of UKESM1
 204 model have shown that the radiative forcing and temperature change are strong func-
 205 tions of altitude, and more weakly dependent on the latitude of the injection (A. C. Jones
 206 et al., 2016, 2017).

207 For G6controller, the majority of the SO₂ is injected at 30°N and 30°S from 2040
 208 onwards and by the end of century only 20% of the total SO₂ is injected at 15°N and 15°S.
 209 This is generally similar to the UKESM1 ARISE-SAI-1.5 simulations described in Henry
 210 et al. (2023), where most of the injection also occurs at the subtropical latitudes (i.e. 30°N
 211 and 30°S). However, a notable difference is that G6controller continues to mostly inject
 212 at these two latitudes throughout the simulation while Henry et al. (2023) report a marked
 213 increase in injection at 15°N halfway through their simulation. This is likely partly due
 214 to the differences in the underlying scenarios (i.e. SSP5-8.5 here vs SSP2-4.5 in ARISE-
 215 SAI-1.5) which have been found to be important in other SAI simulations (Fasullo & Richter,
 216 2022). The similarity of the large-scale UKESM1 temperature responses to injections at
 217 15°N and 30°N determined from the 10-year long sensitivity runs used to train the con-
 218 troller (Visioni, Bednarz, et al., 2023) can lead to relatively large changes in the controller's

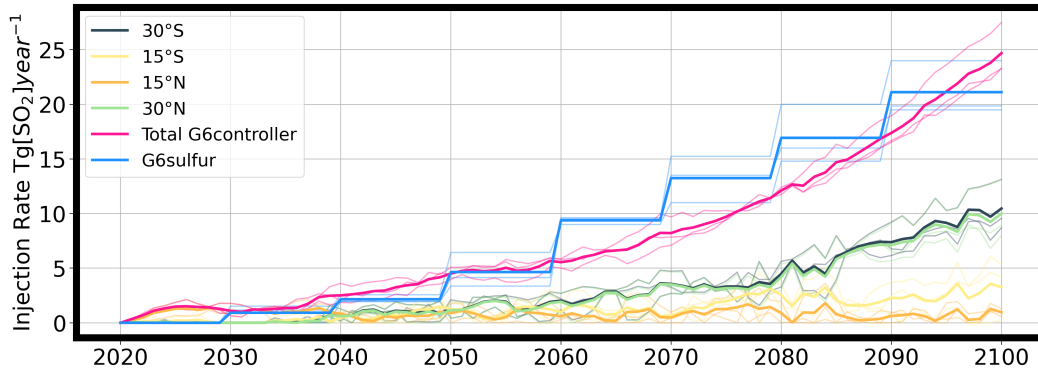


Figure 1. Annual injection rates ($\text{Tg}[\text{SO}_2]\text{year}^{-1}$) for G6sulfur (blue) and G6controller (pink), with the injections at each individual latitude in G6controller shown in other colours. The thick lines represent the ensemble mean, whereas thin lines show each ensemble member.

219 partitioning of injections over these latitudes under comparatively small changes in the
 220 underlying climate.

221 Figure 2 shows how each strategy performs over the 80 years of the simulations with
 222 respect to the three temperature targets; global mean surface air temperature (T_0), the
 223 interhemispheric temperature gradient (T_1) and the equator-to-pole gradient (T_2). These
 224 targets correspond to the values simulated in the SSP2-4.5 warming scenario, as per the
 225 G6 scenario design. As seen in Fig 2a, both simulations reduce the global mean surface
 226 air temperature by 3°C by the end of the century. G6controller is also designed to meet
 227 T_1 and T_2 . Whilst the G6sulfur strategy was not designed to meet the T_1 temperature
 228 target, both injection strategies in fact meet this target relatively well. This was also true
 229 in CESM1 (Kravitz et al., 2019) however, similar simulations in CESM2 do not meet the
 230 T_1 target (Zhang et al., 2023), suggesting that this result is model dependent.

231 Regarding T_2 , SSP5-8.5 shows a substantial decrease in the magnitude of the (neg-
 232 ative) equator-to-pole gradient over the 21st century, which is caused by the strong arctic
 233 amplification commonly found in UKESM1 under increasing greenhouse gas (GHG)
 234 emissions (e.g. (Swaminathan et al., 2022; Henry et al., 2023)). G6controller meets the
 235 T_2 target relatively well during the first 60 years of the simulation, although a small bias
 236 emerges over the final 20 years. In comparison, G6sulfur, which was not designed to meet
 237 the T_2 target, presents a similar significant decrease in the magnitude of the equator-
 238 to-pole gradient to the SSP5-8.5 warming scenario.

239 The driving factor in the reduction in the magnitude of the equator-to-pole tem-
 240 perature gradient in G6sulfur compared to G6controller is the difference in the distri-
 241 bution of stratospheric aerosol. Figure 3a shows the end of the century zonal stratospheric
 242 aerosol optical depth (sAOD) in both G6sulfur and G6controller. The sAOD in G6sulfur
 243 is mainly confined to the tropical region with limited dispersion towards the poles as aerosols
 244 are confined inside the tropical pipe. As such, the peak sAOD values (0.45) simulated
 245 in the narrow band around the equator are over double those seen at high latitudes. In
 246 contrast, stratospheric aerosols are much more dispersed under G6controller, with sub-
 247 stantially higher sAOD values over the midlatitudes and the poles.

248 Model intercomparisons have previously highlighted a stronger confinement of aerosols
 249 in the tropical stratosphere in UKESM1 compared to other models (Visioni et al., 2021;
 250 Visioni, Bednarz, et al., 2023; Bednarz, Visioni, Kravitz, et al., 2023). Between 10°N and
 251 10°S the sAOD in G6sulfur is over four times greater than G6controller whilst at most

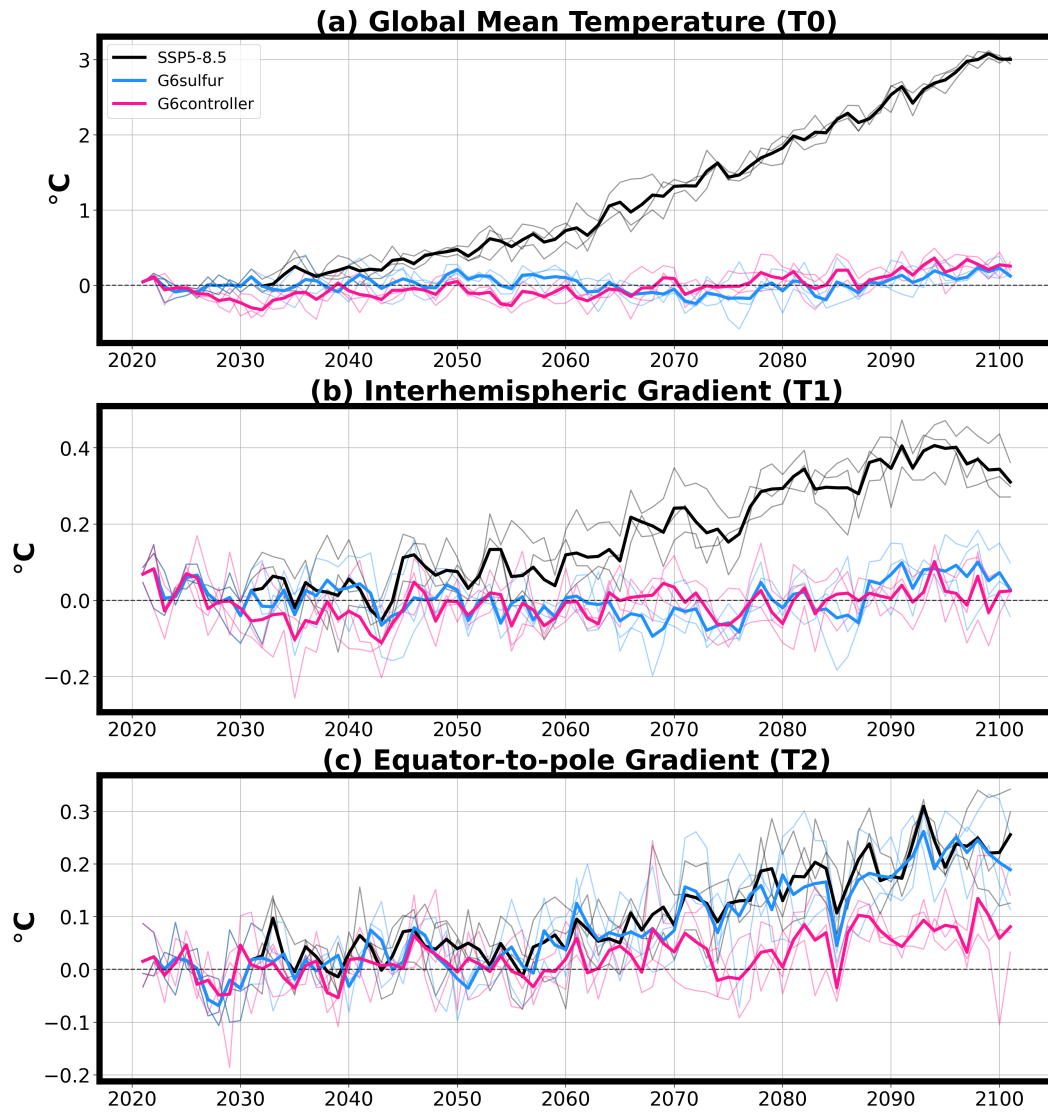


Figure 2. Changes in annual mean (a) global mean temperature, T0 (b) interhemispheric gradient, T1 (c) equator-to-pole gradient, T2 for SSP5-8.5 (black), G6sulfur (blue), G6controller (pink) compared to those in the SSP2-4.5 scenario. The thick lines represent the ensemble mean, whereas thin lines show each ensemble member.

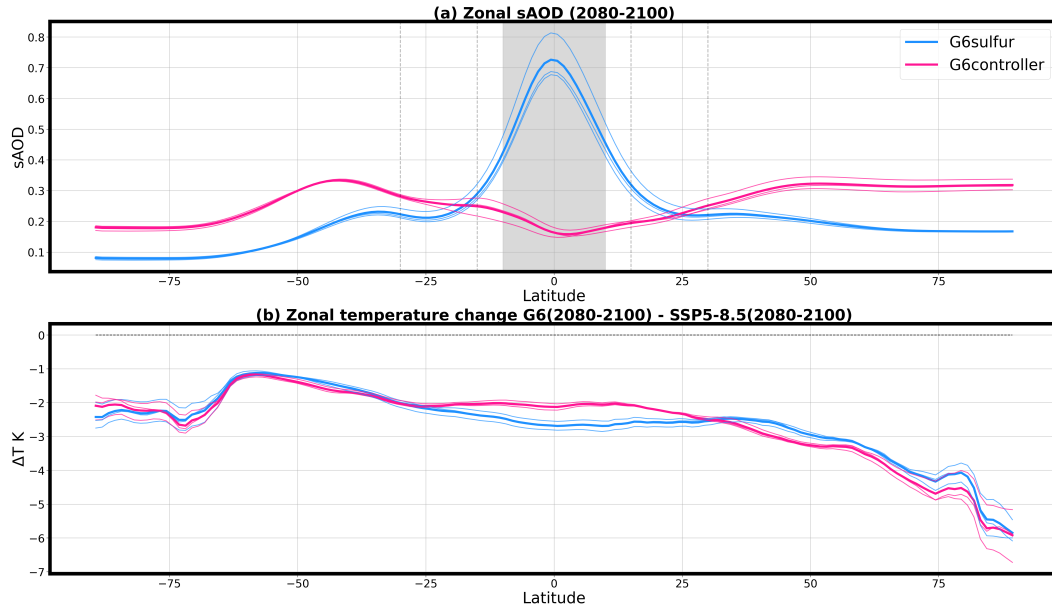


Figure 3. (a) Zonal mean stratospheric aerosol optical depth in G6sulfur (blue) and G6controller (pink). The shaded region between 10°N and 10°S represents the injection location for G6sulfur and the vertical dashed lines at 30°S, 15°S, 15°N and 30°N show the injection locations for G6controller. (b) Zonal mean temperature changes in G6sulfur (blue) and G6controller (pink) relative to the SSP5-8.5 scenario. The thick lines represent the ensemble mean, whereas thin lines show each ensemble member.

252 other latitudes the sAOD in G6sulfur is only around half of that in G6controller (Fig-
 253 ure 3a). Despite substantial differences in the latitudinal distribution of aerosols and sAOD,
 254 the overall latitudinal pattern of cooling is similar in the two injection strategies (Fig-
 255 ure 3b), with the greatest cooling simulated in the Arctic. Whilst the overall cooling re-
 256 sponse is similar in both simulations relative to the SSP5-8.5 scenario, there are signif-
 257 icant differences between injection strategies in surface temperature relative to the tar-
 258 get, SSP2-4.5, scenario. This supports results from Henry et al. (2023) indicating that
 259 the latitudinal pattern of the SAI-induced surface cooling relative to the baseline sce-
 260 nario in UKESM is not dominated by the latitudinal pattern of the direct radiative forc-
 261 ing from stratospheric aerosol but rather this model's internal climate feedbacks.

262 4 Surface air temperature changes

263 Even though both injection strategies meet the same global mean near-surface air
 264 temperature target, large differences in the regional temperature response between the
 265 SSP2-4.5 and SAI scenarios are simulated, in agreement with the previous CESM SAI
 266 studies (e.g., (Kravitz et al., 2019; Zhang et al., 2023)). This is illustrated in Fig. 4 with
 267 the significant differences between the end of the century (2081 - 2100) G6 and SSP2-
 268 4.5 temperatures across the two injection strategies. Under G6sulfur, the large strato-
 269 spheric aerosol burden across the equatorial region results in a tropical cooling relative
 270 to SSP2-4.5 exceeding 1.5°C in places. There is also a residual warming in the polar re-
 271 gions, in some places exceeding 1.5°C, with greater warming seen in the Arctic than the
 272 Antarctic. As aforementioned, this regional disparity drives the weakening of the equator-
 273 to-pole gradient (i.e. an increase in T_2 in Fig. 2c) under an equatorial injection.

274 Under the multi-latitude injection strategy, G6controller, the sAOD is more evenly
 275 distributed across both hemispheres (Fig. 3a) and results in a more homogeneous tem-
 276 perature response. There are fewer AR6 regions (12% G6controller versus 25% G6sulfur)
 277 which experience a significant cooling relative to SSP2-4.5 (Fig. 4c). Nonetheless, a sim-
 278 ilar pattern of residual warming is found across the poles, especially in the Arctic, al-
 279 though reduced in magnitude. Additionally, G6controller is unable to cool the Amazon
 280 (NSA, NES, SAM) to within the range of variability (± 1 std) of the target, whereas G6sulfur
 281 does. This is in part due to a greater warming in this region under SSP5-8.5 that can-
 282 not be fully mitigated under this SAI strategy (Fig. 4c, Fig. S2), and the comparatively
 283 lower sAOD in G6controller over this region compared to G6sulfur (Figure S3).

284 Figure 4c highlights the regions where the surface air temperature over land is out-
 285 side of the range of variability (± 1 std) of the SSP2-4.5 warming scenario (as illustrated
 286 by grey lines). In both strategies the AR6 regions across northern Eurasia (EEU, RAR,
 287 WSB, ESB, RFE for G6sulfur; RAR, ESB, RFE for G6controller) exceed this thresh-
 288 old, owing to the high arctic amplification in UKESM1 under the SSP5-8.5 GHG sce-
 289 nario that cannot be fully mitigated with these SAI strategies (see also (Pan et al., 2023;
 290 Swaminathan et al., 2022)).

291 In addition, in G6controller half of the AR6 regions experiencing statistically sig-
 292 nificant temperature changes also experience a particularly strong regional warming un-
 293 der SSP5-8.5 (e.g. North America (NWN), central South America (SAM), and north-
 294 ern Russia (RAR, ESB, RFE); Figure 4c) that is not fully offset under SAI in this strat-
 295 egy. For G6sulfur, on the other hand, these regions are more widespread and largely lo-
 296 cated in the tropics as a result of the “overcooling” from the high stratospheric aerosol
 297 burden. Henry et al. (2023) found a similar temperature response to those seen in G6controller,
 298 noting that the Arctic warming occurs mostly in winter (DJF) ((Henry et al., 2023); Fig-
 299 ure S3).

300 It is clear from Fig. 4 that a multi-latitude injection strategy such as G6controller
 301 is better able to balance the “overcooling” that has been previously observed from the
 302 early equatorial SAI strategies (e.g., (Kravitz et al., 2013, 2019; Laakso et al., 2017)) and
 303 is able to reduce residual warming of the poles. Unlike the previous studies, however,
 304 we have also shown that this strategy leads to the undercooling of the Amazon and, to
 305 a lesser extent, the undercooling of land regions of the maritime continent in UKESM1.

306 5 Changes in precipitation and its drivers

307 5.1 Precipitation response

308 In general, changes in global mean precipitation tend to scale with changes in tem-
 309 perature. While the global mean temperatures in G6sulfur and G6controller are, by de-
 310 sign, maintained at SSP2-4.5 levels, global mean precipitation is reduced compared to
 311 SSP2-4.5. Previous studies have shown that SAI exhibits a different hydrological sensi-
 312 tivity to greenhouse gas forcings (e.g. (Bala et al., 2008; Niemeier et al., 2013; Klei-
 313 don et al., 2015) and that changes in both large scale and regional tropospheric circu-
 314 lation (e.g. (Cheng et al., 2022; Simpson et al., 2019)) and the combined effects of these
 315 on the hydrological cycle and regional precipitation are uncertain (Tilmes et al., 2013;
 316 Ricke et al., 2023). Our results show that global mean precipitation under both G6 strate-
 317 gies increases at a similar rate to SSP2-4.5 for the first 30 years of the simulations but
 318 subsequently diverge. The global mean precipitation under G6sulfur decreases slightly
 319 post 2050 and then stabilises for the final 30 years, whilst under G6controller it contin-
 320 ues to increase throughout the 21st century albeit at a slower rate than in SSP2-4.5. Av-
 321 eraged over the last two decades (2080-2100) this corresponds to the global mean decrease
 322 of 0.14 mm day^{-1} (- 4%) for G6sulfur and 0.09 mm day^{-1} (- 2.7%) for G6controller re-
 323 lative to SSP2-4.5 in the same period (Figure ??a).

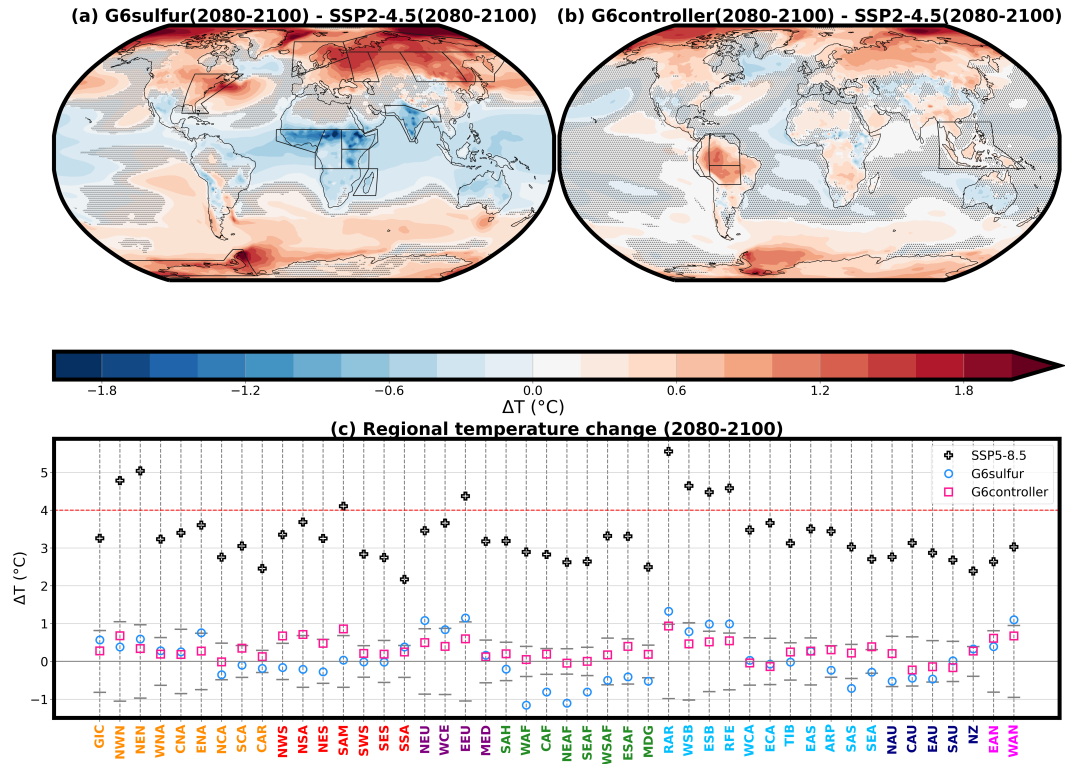


Figure 4. (a-b) Annual surface air temperature change in the ensemble-mean averaged over 2080-2100 for (a) G6sulfur and (b) G6controller relative to the SSP2-4.5 ensemble mean in the same time period. Regions outlined in black represent the AR6 land-only regions where the surface air temperature change was greater than one standard deviation in SSP2-4.5. Shaded areas indicate where the difference is not statistically significant, as evaluated using a double-sided t-test with $p < 0.05$ considering all ensemble members and 20 years as independent samples. (c) Regional temperature change relative to SSP2-4.5 (grey lines 1std SSP2-4.5, red dashed line 4°C)

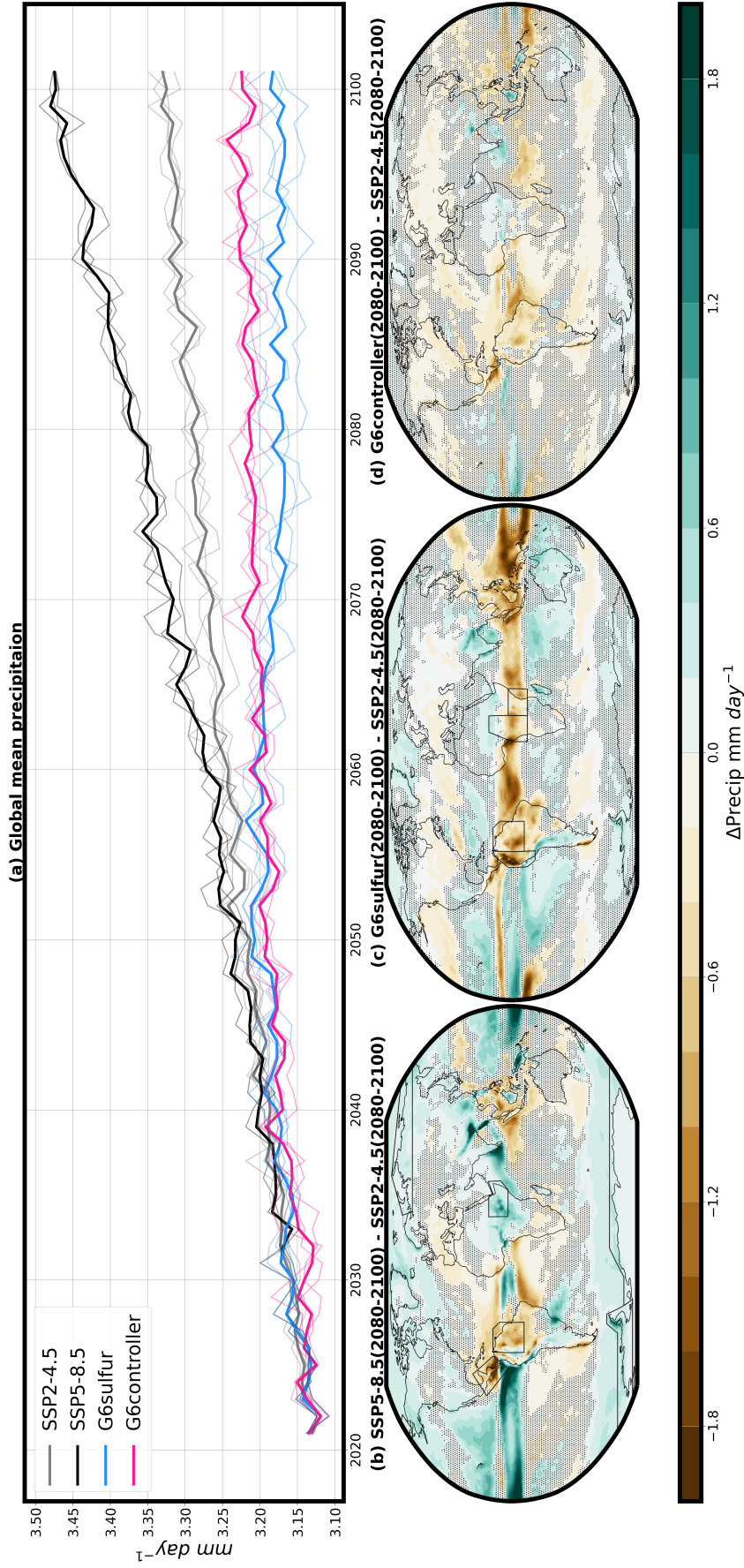


Figure 5. (a) Global mean precipitation for SSP2-4.5 (grey), SSP5-8.5 (black), G6sulfur (blue) and G6controller (pink). The thick lines represent the ensemble mean, whereas thin lines show each ensemble member. (b-d) Annual precipitation change in the ensemble-mean averaged over 2080-2100 for (b) SSP5-8.5, (c) G6sulfur and (d) G6controller relative to the SSP2-4.5 ensemble mean in the same time period. Regions outlined in black represent the AR6 land-only regions where the change in precipitation was greater than one standard deviation in SSP2-4.5. Shaded areas indicate where the difference is not statistically significant, as evaluated using a double-sided t-test with $p < 0.05$ considering all ensemble members and 20 years as independent samples.

324 Similarly to the surface air temperature response, the regional pattern of precip-
 325 itation change is heterogeneous. Figure ??b-d shows the end of the century (2080-2100)
 326 mean precipitation relative to SSP2-4.5 for SSP5-8.5, G6sulfur and G6controller. In the
 327 high emissions scenario, SSP5-8.5, whilst global mean precipitation increases, there is
 328 a significant decrease in precipitation over the Amazon region and over southern Europe.
 329 Regions which experience the largest mean increase in precipitation relative to SSP2-
 330 4.5 include East Africa, the Tibetan Plateau and Indonesia. As in Figure 4, land regions
 331 outside of the range of variability ($\pm 1\text{std}$) of SSP2-4.5 have been highlighted.

332 As expected from the global mean, G6sulfur shows large areas of decreased precip-
 333 itation, mainly throughout the tropical region but also across large areas of Eurasia
 334 and North America. The reduction of precipitation around the equator in G6sulfur, ac-
 335 companied by the increase in precipitation in the subtropics, reflects a weakening of the
 336 intensity of Hadley Circulation (Section 5.2). This weakening is one of the key drivers
 337 in the greater reduction of precipitation over the Amazon in G6sulfur compared to that
 338 under SSP5-8.5 and G6controller. The distribution of sAOD in G6sulfur (Figure S1), com-
 339 pared to G6controller, results in a strong reduction in surface solar radiation across the
 340 tropics. This reduces the surface sensible and latent heat fluxes, increasing the stabili-
 341 ty of the atmosphere and inhibiting convection, contributing to the weakening of the
 342 Hadley Circulation and therefore a reduction in tropical precipitation (Schneider et al.,
 343 2010).

344 Changes in precipitation under G6controller are found to be smaller compared to
 345 G6sulfur, with less statistical significance over both land ocean regions and with fewer
 346 AR6 regions outside the range of variability in SSP2-4.5 (black boxes in Fig. ??b-d). While
 347 the G6controller strategy does show some statistically significant increases in precipi-
 348 tation over Bangladesh, the increase is much reduced compared to that found in either
 349 SSP5-8.5 or G6sulfur. The spatial pattern of precipitation change over land in G6controller
 350 is mostly similar to that of G6sulfur but is of a smaller magnitude. An exception to this
 351 are the precipitation changes over the Maritime Continent, whereby precipitation decreases
 352 over land in this region in G6sulfur by 0.58 mm day^{-1} but increases in G6controller by
 353 0.17 mm day^{-1} .

354 G6controller was designed to minimise changes in the interhemispheric tempera-
 355 ture difference (T_1) to minimise large scale shifts in the ITCZ (e.g. (J. M. Haywood et
 356 al., 2013)) that are controlled by the strength of the cross-equatorial flows of energy and
 357 moisture (e.g. (Frierson et al., 2013)). G6sulfur also meets this target despite no explicit
 358 design choice (Figure 2b), however there are greater differences in the precipitation re-
 359 sponse under G6sulfur, especially in the tropical region. This can be examined further
 360 by looking at the seasonal precipitation cycle and changes to large-scale tropospheric cir-
 361 culations.

362 For many regions, especially in the tropics, the seasonal precipitation change is more
 363 relevant than the annual mean owing to the influence of the seasonal monsoons. Figure
 364 6 shows the end of century (2080-2100) seasonal (December, January, February (DJF);
 365 June, July, August (JJA)) precipitation change relative to SSP2-4.5 for SSP5-8.5, G6sulfur
 366 and G6controller. An increase in precipitation over the Maritime Continent in DJF and
 367 over the Tibetan Plateau in JJA dominates the signal in SSP5-8.5. The decrease in pre-
 368 cipitation over the Amazon mostly occurs during DJF, the southern hemisphere sum-
 369 mer. This feature is also seen in both G6 strategies, however in G6sulfur the decrease
 370 (1.05 mm day^{-1}) is double that of both SSP5-8.5 (0.50 mm day^{-1}) and G6controller (0.58
 371 mm day^{-1}). In G6sulfur the reduction in tropical precipitation is greater in DJF than
 372 JJA and reflects changes to the Hadley circulation (Section 5.2). Similarly to the annual
 373 mean, changes to seasonal precipitation in G6controller are much smaller and less sig-
 374 nificant.

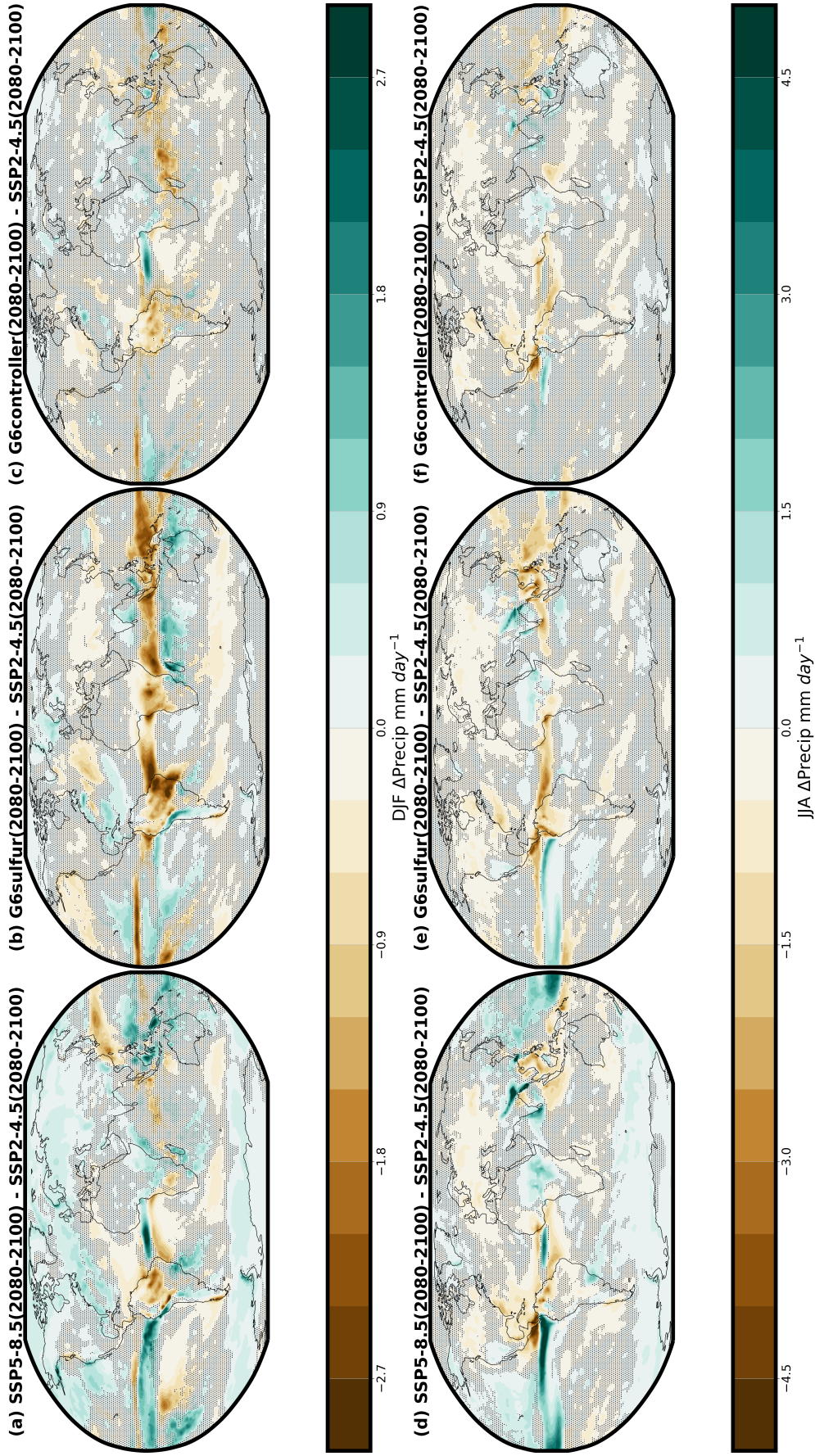


Figure 6. Seasonal precipitation change in the ensemble-mean averaged over December, January, February (DJF) and June, July, August (JJA) 2080-2100 for (a, d) SSP5-8.6, (b, e) G6sulfur and (c, f) G6controller relative to the SSP2-4.5 ensemble mean in the same time period. Regions outlined in black represent the AR6 land-only regions where the change in precipitation was greater than one standard deviation in SSP2-4.5. Shaded areas indicate where the difference is not statistically significant, as evaluated using a double-sided t-test with $p < 0.05$ considering all ensemble members and 20 years as independent samples.

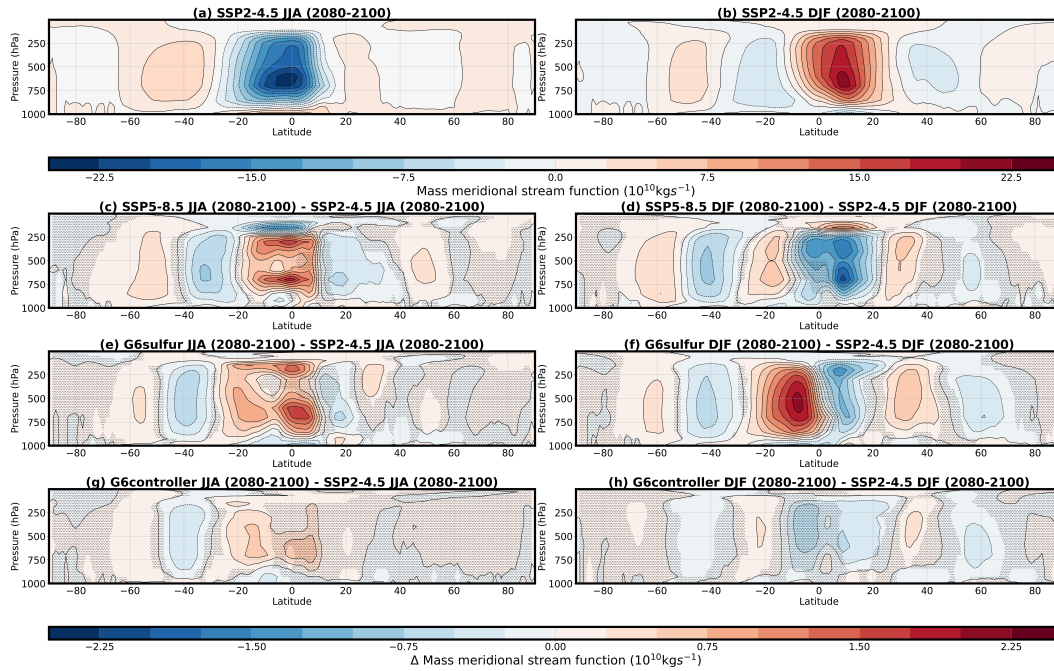


Figure 7. Zonal and ensemble mean meridional mass stream function (1010kg s^{-1}) in JJA (a, c, e, g) and DJF (b, d, f, h) averaged over the years 2080-2100 for SSP2-4.5 (a, b) and the difference in meridional mass stream function for (c, d) SSP5-8.5, (e, f) G6sulfur and (g, h) G6controller relative to the SSP2-4.5 scenario. Red indicates a clockwise rotation and blue indicates an anticlockwise rotation. Shaded areas indicate where the difference is not statistically significant, as evaluated using a double-sided t-test with $p < 0.05$ considering all ensemble members and 20 years as independent samples.

375

5.2 Large-scale tropospheric circulation changes

376

377

378

379

380

381

382

383

384

385

386

387

388

389

The Hadley Circulation (HC) is a large-scale tropical atmospheric circulation with rising air at the equator diverging poleward in the upper troposphere and descending in the subtropics. The structure and behaviour of the HC can greatly influence global climate, playing an important role in forming tropical and subtropical climatic zones. The warm and humid converging air in the ascending branches of the HC forms the ITCZ, with its associated heavy precipitation, whilst the sinking branches consist of mainly dry air and, thus, are associated with little rainfall, resulting in large arid regions within the subtropics. Some studies have reported a weakening in the HC intensity with increased GHGs (e.g., (Lu et al., 2007; Ma et al., 2012)) although Vallis et al. (2015) found some disagreement within CMIP5 models in the southern hemisphere HC during JJA and observations show a poleward expansion of the circulation (Staten et al., 2018; Waugh et al., 2018). Since changes to precipitation patterns in the tropics could have large impacts on food and water security for many people (Wheeler & Von Braun, 2013), it is important to assess how SAI could impact these circulation changes.

390

391

392

393

394

395

To assess changes in the HC intensity under the GHG induced warming and the SAI scenarios we calculate the meridional mass stream function following the formula in Haigh et al. (2005). SSP2-4.5 shows the typical anticlockwise rotation in the southern hemisphere cell and a clockwise rotation in the northern hemisphere cell, with both the position and intensity of the two cells varying between winter and summer (Figure 7a,b).

Figure 7c-h shows the difference in the DJF and JJA meridional mass stream function relative to SSP2-4.5 for SSP5-8.5, G6sulfur and G6controller. SSP5-8.5 shows a significantly weaker HC in both hemispheres compared to SSP2-4.5, which is consistent with the literature (e.g. (Vallis et al., 2015)). In DJF, G6sulfur shows a significant change to the northern HC cell compared to SSP2-4.5, with the amplitude of the stream function maximum at 500 hPa decreasing by 5%. This is associated with a significant reduction (20%) of the vertical velocity at the equator, contributing to the reduction of precipitation in the tropical region (Figure 6b), and a significant increase in vertical velocity (9%) around the downward branch (not shown). We also note that the descending branch of the northern HC shifts poleward, therefore widening the HC and shifting the subtropical dry zone polewards, contributing to the significant decrease in precipitation around continental Asia (Fig. 6b). In contrast, while some weakening of the northern HC occurs in DJF under G6controller, the response is much weaker and not significant.

In JJA the response under G6controller is similar to the DJF response, i.e. a slight decrease of HC intensity with little statistical significance in the upward branch. Under G6sulfur we see a similar response to that of SSP5-8.5 with a decrease in HC intensity, although unlike the DJF response there is little change in the width of the HC.

Changes in the HC intensity are often explained in terms of the associated changes in meridional temperature gradients, troposphere static stability and tropopause height (e.g. (Held, 2000; Seo et al., 2014)). As we discussed in Section 3, the meridional temperature gradient in G6controller is relatively well maintained throughout the simulations compared to the equatorial injection strategy G6sulfur which was not designed to meet this target and thus results in the anomalous weakening of the gradient of around 0.2°C relative to the target by the end of the century. In addition, the magnitude of the deceleration in upwelling in the tropical troposphere is smaller in G6controller than in G6sulfur. This deceleration is caused by an increase in static stability associated with lower stratospheric heating and tropospheric cooling which occurs in the tropics G6sulfur but less so in G6controller (Figure 8b-c). Finally, changes in the tropical tropospheric and lower stratospheric temperatures in G6sulfur lead to the lowering of the tropopause height compared to the SSP2-4.5 target, the magnitude of which becomes much smaller in G6controller (Fig. 8d), we see a 10% decrease in the altitude of the tropopause height between G6sulfur and G6controller, with only a very small decrease (3.5%) between G6controller and the target, SSP2-4.5.

These results agree with other studies assessing changes to the HC under different injection strategies (Cheng et al., 2022; Bednarz, Butler, et al., 2023). Cheng et al. (2022) compared HC intensity in the CESM1 simulations in the GLENS and the equivalent equatorial injection strategy defined in Kravitz et al. (2019) and Bednarz, Butler, et al. (2023) compared an equatorial injection with multiple symmetric off-equatorial strategies in CESM2, with both studies reporting a similar result.

We note that SAI-induced changes in surface energy fluxes are only one of the possible drivers of the simulated large-scale circulation and precipitation changes, and their dependence on the SAI strategy. Simpson et al. (2019) examined the precipitation response to stratospheric heating in the CESM1 model and found some significant changes, particularly in tropical precipitation with wet regions getting drier and dry regions getting wetter, suggesting that the top-down influence of the SAI-induced lower stratospheric heating on tropospheric circulation and precipitation could also play a role here. Note that Simpson et al. (2019) apply a tropical stratospheric heating that is approximately twice as strong as that modelled here in the G6sulfur simulations (Section 6.1), and that they acknowledge that the specific feedback mechanisms linking stratospheric heating to precipitation changes are not well understood.

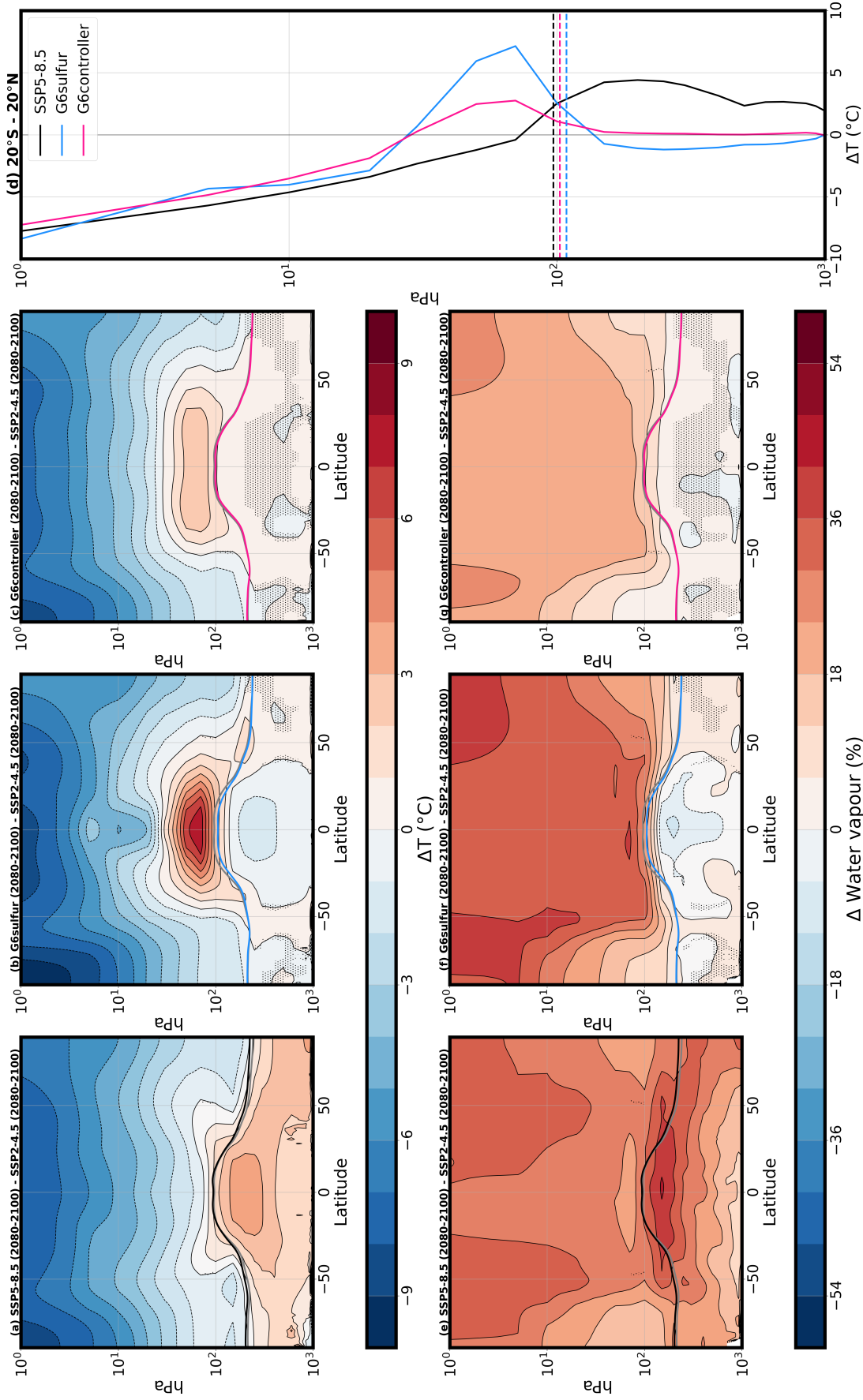


Figure 8. (a-c) Zonal mean temperature change in the ensemble-mean averaged over 2080-2100 for (a) SSP5-8.5, (b) G6sulfur and (c) G6controller relative to the SSP2-4.5 ensemble mean in the same period. (d) Zonal and ensemble mean temperature averaged over 20°S - 20°N and 2080-2100 for SSP5-8.5 (black), G6sulfur (blue) and G6controller (pink) relative to the SSP2-4.5 scenario. (e-f) Zonal mean percentage change of water vapour in the ensemble-mean averaged over 2080-2100 for (e) SSP5-8.5, (f) G6sulfur and (g) G6controller relative to the SSP2-4.5 ensemble mean in the same period. The solid lines on (a, b, c, e, f, g) indicate the tropopause height for SSP2-4.5 (grey), SSP5-8.5 (black), G6sulfur (blue) and G6controller (pink). Shaded areas indicate where the difference is not statistically significant, as evaluated using a double-sided t-test with $p < 0.05$ considering all ensemble members and 20 years as independent samples.

6 Stratospheric response

6.1 Stratospheric temperatures

One of the important impacts of stratospheric aerosol injection to consider is the stratospheric heating induced by the introduction of sulfate aerosols. Since sulfate is not purely scattering at wavelengths longer than approximately 1.4 μm (e.g. (Dykema et al., 2016; J. Haywood et al., 2022)), the partial absorption of solar and terrestrial radiation by aerosols results in stratospheric heating. Previous studies have investigated the role of stratospheric heating in contributing to climate impacts from SAI, including changes in stratospheric and tropospheric circulation and the resulting modulation of global and regional precipitation patterns (Visioni et al., 2020; Cheng et al., 2022; Simpson et al., 2019).

Figure 8a-c shows the difference in zonal mean temperature (2080-2100) relative to SSP2-4.5 for SSP5-8.5, G6sulfur and G6controller. In agreement with previous studies (e.g. (Kravitz et al., 2019; Cheng et al., 2022)), tropospheric temperatures increase under the high GHG scenario (SSP5-8.5), with a maximum in the tropical upper troposphere and a small warming extending up to the tropical lower stratosphere. Both G6 SAI strategies show temperature increases in the extra-polar lower stratosphere, with G6sulfur warming the tropical stratosphere (20°S - 20°N) by 66% more than G6controller (Figure 8d). The larger amplitude of the tropical lower stratospheric heating in G6sulfur compared to G6controller results from the combination of much higher sulfate concentrations simulated within the tropics (Fig. S4; Fig. 3a; see also Kravitz et al. (2019); Bednarz, Butler, et al. (2023)) as well as the lower altitude of SO₂ injection (see also (Lee et al., 2023)).

Warming in the tropical lower stratosphere in both G6 strategies is associated with warming and lowering of the tropical tropopause. This allows for an increase in stratospheric water vapour (Figure 8e-g), which acts to offset the direct aerosol-induced surface cooling (J. M. Haywood et al., 2022; Lee et al., 2023; Bednarz, Butler, et al., 2023) as well as modulating stratospheric temperatures and ozone concentrations (Maycock et al., 2013; Tilmes et al., 2021).

In comparison, the magnitude of the lower stratospheric warming and the resulting increase in stratospheric water vapour in G6controller is much reduced compared to G6solar. The latter is also partially related to the lower altitude of the SO₂ injection in G6solar (18-20 km) compared to G6controller (21.5 km), thereby resulting in larger impacts on tropopause temperatures, in agreement with the results of Lee et al. (2023).

6.2 Stratospheric Ozone

Changes to stratospheric temperatures as a result of SAI can drive changes in stratospheric ozone, due to changes in both stratospheric dynamics and chemistry. Studies have shown that enhancements of the stratospheric sulfate aerosol layer from SAI would increase the aerosol surface area density, influencing halogen activation in the lower stratosphere and the removal of active nitrogen species in the middle stratosphere, thereby modulating chemical ozone loss (J. Haywood et al., 2022; Tilmes, Richter, Kravitz, et al., 2018; Tilmes et al., 2022; Bednarz, Butler, et al., 2023; Bednarz, Visioni, Butler, et al., 2023). In addition, the SAI-induced lower stratospheric heating will also influence ozone via changes in the large scale transport as well as through increased stratospheric water vapour levels and thus chemical ozone loss.

Figure 9(a-c) shows the percentage change of ozone relative to SSP2-4.5 for SSP5-8.5, G6sulfur and G6controller. We see a general decrease of ozone under SSP5-8.5 around the tropopause at most latitudes as the result of the GHG-induced increase in tropopause height relative to SSP2-4.5. Ozone also decreases in SSP5-8.5 in the tropical lower strato-

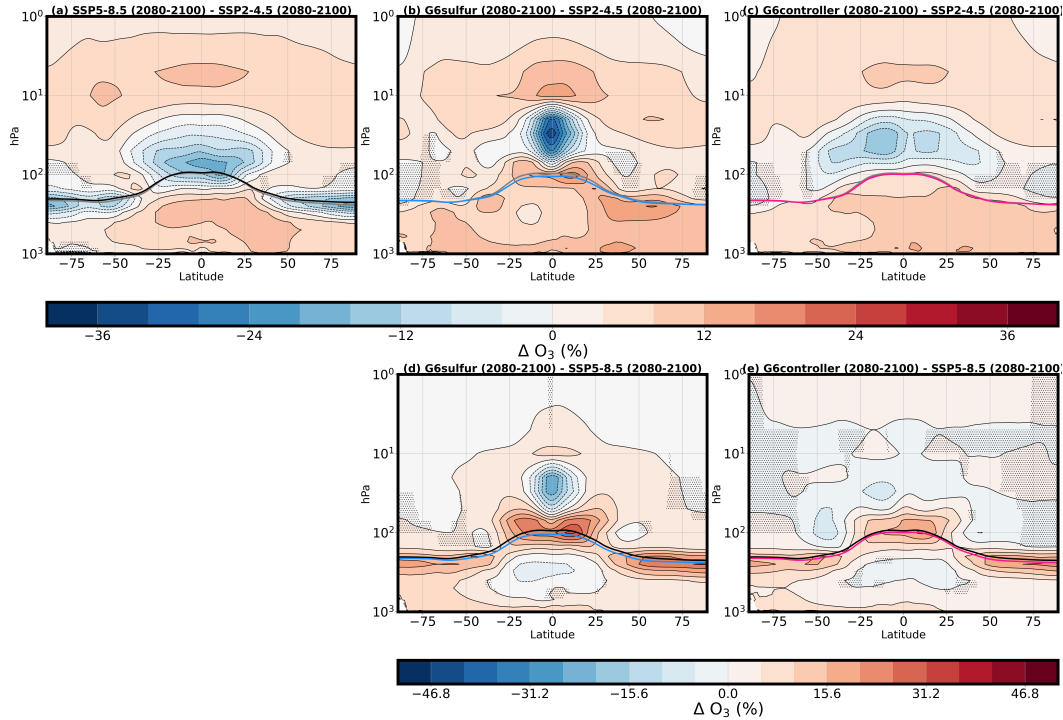


Figure 9. Zonal mean percentage difference of ozone in the ensemble-mean averaged over 2080-2100 for (a) SSP5-8.5, (b) G6sulfur and (c) G6controller relative to SSP2-4.5 in the same period and (d) G6sulfur and (e) G6controller relative to SSP5-8.5 in the same period. The solid lines indicate the tropopause height for SSP2-4.5 (grey), SSP5-8.5 (black), G6sulfur (blue) and G6controller (pink). Shaded areas indicate where the difference is not statistically significant, as evaluated using a double-sided t-test with $p < 0.05$ considering all ensemble members and 20 years as independent samples.

495 sphere, likely as the result of the GHG-induced strengthening of the Brewer Dobson Cir-
 496 culation, and the resulting dynamically-induced ozone reduction as more ozone-poor air
 497 is transported from the troposphere. In addition, higher stratospheric H_2O (Figure 8e)
 498 owing to higher methane emissions in SSP5-8.5 acts to enhance the HOx-mediated chemi-
 499 cal ozone loss throughout the stratosphere, and this effect can thus contribute to the
 500 ozone decrease simulated in the tropical lower stratosphere. In the upper stratosphere,
 501 where chemical timescales are much faster than dynamical timescales, SSP5-8.5 shows
 502 increased ozone throughout the globe compared to the SSP2-4.5. The response results
 503 form the GHG-induced stratospheric cooling and the resulting declaration of the catalytic
 504 chemical ozone loss in that region.

505 In order to isolate the purely SAI-induced response from those arising from the GHG-
 506 induced changes in stratospheric temperatures, chemistry and transport (which was also
 507 evident in the SSP5-8.5 response in Fig. 9a), Figure 9d-e compares the percentage change
 508 of ozone in both G6 strategies relative to SSP5-8.5. Both G6 strategies show significant
 509 ozone increases around the tropopause throughout the globe as the result of the SAI-
 510 induced lowering of the tropopause height (Section 6.1).

511 In G6sulfur, there are also further ozone increases in the subtropical lower strato-
 512 sphere and an ozone decrease in the equatorial stratosphere above it. The response likely
 513 results from the SAI-induced changes in circulation, with the deceleration of the shal-

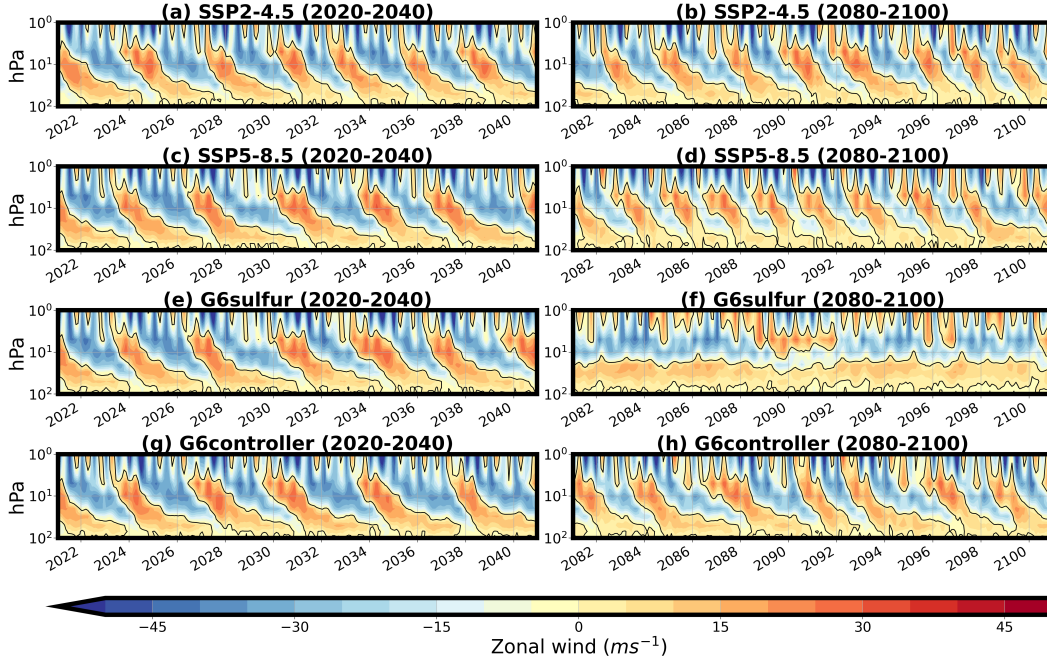


Figure 10. Zonal mean winds of one ensemble member averaged over 5°S - 5°N as a function of time (months) over 2020-2040 (a, c, e, g) and 2080-2100 (b, d, f, h) for (a, b) SSP2-4.5, (c, d) SSP5-8.6, (e, f) G6sulfur and (g, h) G6controller.

514 low branch of the BDC and upwelling in the tropical upper troposphere and lower strato-
 515 sphere (reducing the transport of ozone-poor air into the lower stratosphere) and accel-
 516 eration of the deep BDC branch (enhancing the transport of ozone-poor tropical lower
 517 stratospheric air into the middle stratosphere above the aerosol layer), in a manner sim-
 518 ilar to that in previous CESM studies (Tilmes, Richter, Mills, et al., 2018; Bednarz, But-
 519 ler, et al., 2023). In contrast, these ozone changes are much reduced in G6controller, likely
 520 as the result of the much reduced stratospheric heating (Fig. 8c) and, thus, changes in
 521 stratospheric circulation and transport. As discussed in (J. Haywood et al., 2022), the
 522 spatial distribution of sulfate aerosol strongly influences changes in transport which is
 523 the largest difference between G6sulfur and G6controller in this case.

524 6.3 Quasi-Biennial Oscillation

525 The Quasi-Biennial Oscillation (QBO) is an easterly and westerly oscillation of the
 526 equatorial zonal winds in the tropical stratosphere. Aquila et al. (2014) first reported
 527 changes to the period and amplitude of the QBO under equatorial injections of sulfur
 528 into the stratosphere. They found that for large increases in stratospheric aerosol bur-
 529 den (5Tg SO₂) the QBO would be locked into a permanent westerly phase. This occurs
 530 as the increased stratospheric warming disturbs the thermal wind balance and increases
 531 the residual vertical velocity (Niemeier et al., 2011) resulting in an additional westerly
 532 component of the zonal wind above the heated aerosol layer, and thus delayed descent
 533 of the westerly QBO phase (Figure S5) (Niemeier & Schmidt, 2017; Aquila et al., 2014).
 534 In addition, in the westerly phase of the QBO there is equatorward motion which results
 535 in stronger aerosol confinement in the tropical pipe where mixing is strongly constrained
 536 (Niemeier & Schmidt, 2017; Punge et al., 2009; Visioni et al., 2018).

537 Figure 10 shows the first and last 20 years of the QBO for one ensemble member
 538 of the SSP5-8.5, SSP2-4.5, G6sulfur and G6controller simulations. Under global warm-
 539 ing we see some changes to the period and amplitude of oscillation, in particular the short-
 540 ening of its period, more pronounced under the high emissions scenario SSP5-8.5. Sim-
 541 ilarly to previous studies (Kravitz et al., 2019; Aquila et al., 2014; Bednarz, Butler, et
 542 al., 2023) the strong tropical lower stratospheric warming under G6sulfur leads to lock-
 543 ing of the QBO into a permanent westerly phase by the end of the century (G6sulfur,
 544 Figure 10f, Figure S5). Despite some noticeable changes to the oscillation relative to SSP2-
 545 4.5, including weakening of its amplitude and elongation of its period, the QBO is not
 546 entirely disrupted under G6controller when the aerosol is injected away from the equa-
 547 tor and the tropical lower stratospheric heating is smaller, supporting results from sim-
 548 ilar comparative studies with the CESM model (e.g (Kravitz et al., 2019; Bednarz, Vi-
 549 sioni, Kravitz, et al., 2023).

550 7 Conclusions

551 In this study we have compared the climate impacts of two stratospheric aerosol
 552 injection strategies using UKESM1 earth system model under the GeoMIP G6 scenario,
 553 both reducing global mean near-surface air temperatures from the SSP5-8.5 levels to those
 554 of SSP2-4.5, i.e. by 3°C by the end of the century. G6sulfur, a quasi- equatorial injec-
 555 tion at 18 km between 10°N and 10°S, with the injection amount manually adjusted ev-
 556 ery decade, and G6controller, a feedback-controlled multi-latitude injection strategy (30°S,
 557 15°S, 15°N and 30°N) at 21.5 km with the global mean surface air temperature and the
 558 interhemispheric and equator-to-pole gradients as its targets. Similar comparisons had
 559 previously only been performed in two versions of the same model (CESM1; (Kravitz
 560 et al., 2019); CESM2; (Zhang et al., 2023)). Our study therefore provides insight into
 561 how the climate responds in UKESM1 under these two different injection strategies, al-
 562 lowing us to begin to understand which climate responses are consistent under SAI and
 563 which are more strategy and/or model dependent.

564 G6sulfur exhibits the robust tropospheric temperature response consisting of “over-
 565 cooling” of the tropics and “undercooling” of the poles typical to previous equatorial SAI
 566 strategies (e.g. (Kravitz et al., 2019)). This is a result of the latitudinal distribution of
 567 stratospheric aerosols which are mostly confined inside the tropical pipe with little dis-
 568 persion towards the mid-latitudes. Similar tropical overcooling is not observed under G6controller
 569 which has a more homogenous surface air temperature response relative to the SSP2-
 570 4.5 target. In the high latitudes, however, the latitudinal pattern of surface cooling re-
 571 lative to the baseline scenario SSP5-8.5 is similar in both injection strategies, with the
 572 greatest cooling occurring in the northern high latitudes. Henry et al. (2023) found sim-
 573 ilar results under the ARISE-SAI-1.5 simulations in UKESM1 and suggested that this
 574 surface cooling is more dependent on the model’s climate feedbacks rather than latitu-
 575 dinal distribution of the direct radiative forcing, a result that is consistent across injec-
 576 tion strategies in this model.

577 There is a widely acknowledged disagreement among climate models regarding re-
 578 gional precipitation changes in a warming climate (Masson-Delmotte et al., 2021). This
 579 disparity significantly contributes to the range of projections concerning both large-scale
 580 and regional changes in the water cycle. Therefore, the impact of SAI on regional and
 581 extreme precipitation is still very uncertain (Ricke et al., 2023), however our results are
 582 consistent with previous studies which suggest that global-mean precipitation is suppressed
 583 under SAI compared to that in the target period. Furthermore, there is a greater reduc-
 584 tion in the global and tropical precipitation under G6sulfur than under G6controller, po-
 585 tentially impacting the water and food security of many people living in these regions
 586 (Wheeler & Von Braun, 2013). There are several contributing factors to the decrease in
 587 tropical precipitation, some of which are still poorly understood. Our analysis suggests
 588 that under G6sulfur the larger decrease in downward shortwave radiation in the trop-

ics compared to G6controller could certainly contribute to the weakening of the Hadley Circulation and thus suppress precipitation in e.g. the Amazon or central African region through changes in the surface energy budget, although dynamically induced changes in tropospheric circulation could also play a role (e.g. (Simpson et al., 2019)). However, it is important to note that significant differences in the sign of tropical precipitation change between CESM2 and UKESM1 have been observed, specifically over India and the Tibetan Plateau (see Figures 6 and 8, (Henry et al., 2023)) which highlights the need for more model intercomparisons and more in depth mechanistic understanding of the key processes involved to determine what would be a robust hydrological response to SAI. Whilst efforts were made to further investigate the role of stratospheric heating on precipitation in the G6 scenarios using idealised simulations, this is an area outside of the scope of this study and will be pursued in future work.

The role of stratospheric heating in the climate response to SAI is complex and needs to be better understood to reduce uncertainty in the model's response. This study showed that the choice to move the injection location away from equator can decrease tropical stratospheric heating by 66% and therefore reduce the impact on the large scale atmospheric dynamics, including the Hadley Circulation (Cheng et al., 2022) and the Quasi-Biennial Oscillation (Kravitz et al., 2019). Our results showed a significant change to the northern and southern hemisphere HC in G6sulfur with poleward shifts of the northern downward branch and a significant weakening of intensity in both hemispheres. Results from G6controller revealed that the weakening of the Hadley cells under SSP5-8.5 could be reduced under this injection strategy. We also showed that the increased stratospheric heating in G6sulfur compared to G6controller contributed to the locking of the westerly phase of the QBO, similar to previous studies (e.g., (Aquila et al., 2014; Kravitz et al., 2019)).

The results of this study highlight the effectiveness of the 4-latitude injection strategy, G6controller, in reducing global mean temperatures by 3°C, whilst mitigating the negative consequences associated with equatorial injection strategies, such as G6sulfur. Although the targets T_0 , T_1 , and T_2 of the G6controller are temperature-based, the benefits of the control algorithm extend beyond temperatures due to associated dynamical feedbacks. Specifically, (i) tropical precipitation is less impacted, due to more limited effects on the Hadley circulation, (ii) the tropical stratosphere warms less, leading to less impact on tropical stratospheric ozone concentrations, and (iii) the reduction in tropical stratospheric heating under G6controller minimises impacts on the Quasi-Biennial Oscillation.

While similar comparisons have been made in other climate models, a comprehensive analysis of an off-equatorial injection strategy across multiple modelling centres is essential to identify commonalities and uncertainties. It's worth noting that the latitudinal injection strategy determined by the controller differs significantly from that of Henry et al. (2023), where the T_0 , T_1 , and T_2 targets were fixed at +1.5°C above model pre-industrial conditions, without temporal target evolution. Furthermore, even with the same scenario and climate targets, injection strategies needed to achieve those targets vary significantly across different climate models, as highlighted by Henry et al. (2023). Determining which strategy best represents the real world remains an open question, emphasising the need for further research in SAI to unravel the complexities and interplay between SAI emissions, forcing patterns, and climate responses. Future work will delve into the differences in extreme events between the two G6 strategies and explore the role of stratospheric heating in G6sulfur.

8 Open Research

The processed model output used throughout this work are available on Zenodo ((Wells, Jones, & Dalvi, 2023); <https://doi.org/10.5281/zenodo.10302574>) and code

640 for reproducibility is available on GitHub ((Wells, Henry, & Bednarz, 2023); <https://doi.org/10.5281/zenodo.10302916>).

642 Acknowledgments

643 Alice Florence Wells, James Matthew Haywood, Matthew Henry, Andy Jones, and Mohit Dalvi were supported by SilverLining through its Safe Climate Research Initiative.
 644 James Matthew Haywood, Andy Jones, and Mohit Dalvi were also supported by the Met
 645 Office Hadley Centre Climate Programme funded by DSIT. James Matthew Haywood
 646 and Matthew Henry were further supported by the NERC EXTEND project (NE/W003880/1).
 647 Alice Florence Wells was further supported by a UKRI Centre for Doctoral Training in
 648 Environmental Intelligence PhD studentship hosted by the University of Exeter. Sup-
 649 port for Ewa M. Bednarz has been provided by the National Oceanic and Atmospheric
 650 Administration (NOAA) cooperative agreement NA22OAR4320151, and the Earth Ra-
 651 diative Budget initiative. Support for Douglas G. MacMartin has been provided by the
 652 Atkinson Center for Sustainability at Cornell University and the National Science Founda-
 653 tion through agreement CBET-2038246.
 654

655 References

- 656 Aquila, V., Garfinkel, C. I., Newman, P., Oman, L., & Waugh, D. (2014). Modi-
 657 fications of the quasi-biennial oscillation by a geoengineering perturbation of
 658 the stratospheric aerosol layer [Journal Article]. *Geophysical Research Let-*
 659 *ters*, *41*(5), 1738-1744. Retrieved from [https://agupubs.onlinelibrary](https://agupubs.onlinelibrary.wiley.com/doi/abs/10.1002/2013GL058818)
 660 [.wiley.com/doi/abs/10.1002/2013GL058818](https://agupubs.onlinelibrary.wiley.com/doi/abs/10.1002/2013GL058818) doi: [https://doi.org/10.1002/](https://doi.org/10.1002/2013GL058818)
 661 [2013GL058818](https://doi.org/10.1002/2013GL058818)
- 662 Archibald, A. T., O'Connor, F. M., Abraham, N. L., Archer-Nicholls, S., Chipper-
 663 field, M. P., Dalvi, M., ... Zeng, G. (2020). Description and evaluation of
 664 the ukca stratosphere-troposphere chemistry scheme (strattrop vn 1.0) imple-
 665 mented in ukesm1 [Journal Article]. *Geoscientific Model Development*, *13*(3),
 666 1223-1266. doi: 10.5194/gmd-13-1223-2020
- 667 Bala, G., Duffy, P. B., & Taylor, K. E. (2008). Impact of geoengineering
 668 schemes on the global hydrological cycle [Journal Article]. *Proceedings*
 669 *of the National Academy of Sciences*, *105*(22), 7664-7669. Retrieved
 670 from <https://www.pnas.org/doi/abs/10.1073/pnas.0711648105> doi:
 671 [doi:10.1073/pnas.0711648105](https://doi.org/10.1073/pnas.0711648105)
- 672 Bednarz, E. M., Butler, A. H., Visioni, D., Zhang, Y., Kravitz, B., & MacMartin,
 673 D. G. (2023). Injection strategy - a driver of atmospheric circulation and ozone
 674 response to stratospheric aerosol geoengineering [Journal Article]. *EGUsphere*,
 675 *2023*, 1-32. Retrieved from [https://egusphere.copernicus.org/preprints/](https://egusphere.copernicus.org/preprints/2023/egusphere-2023-495/)
 676 [2023/egusphere-2023-495/](https://egusphere.copernicus.org/preprints/2023/egusphere-2023-495/) (EGUsphere) doi: 10.5194/egusphere-2023-495
- 677 Bednarz, E. M., Visioni, D., Butler, A. H., Kravitz, B., MacMartin, D. G., &
 678 Tilmes, S. (2023). Potential non-linearities in the high latitude circulation
 679 and ozone response to stratospheric aerosol injection. *Geophysical Research*
 680 *Letters*, *50*(22), e2023GL104726.
- 681 Bednarz, E. M., Visioni, D., Kravitz, B., Jones, A., Haywood, J. M., Richter, J.,
 682 ... Braesicke, P. (2023). Climate response to off-equatorial stratospheric
 683 sulfur injections in three earth system models-part 2: Stratospheric and free-
 684 tropospheric response [Journal Article]. *Atmospheric Chemistry and Physics*,
 685 *23*(1), 687-709.
- 686 Best, M. J., Pryor, M., Clark, D., Rooney, G. G., Essery, R., Ménard, C., ... Ged-
 687 ney, N. (2011). The joint uk land environment simulator (jules), model
 688 description-part 1: energy and water fluxes [Journal Article]. *Geoscientific*
 689 *Model Development*, *4*(3), 677-699.
- 690 Budyko, M. I. (1977). On present-day climatic changes [Journal Article]. *Tellus*,

- 691 29(3), 193-204.
- 692 Cheng, W., MacMartin, D. G., Kravitz, B., Visioni, D., Bednarz, E. M., Xu,
693 Y., ... Deng, X. (2022). Changes in hadley circulation and intertropical
694 convergence zone under strategic stratospheric aerosol geoengineering
695 [Journal Article]. *npj Climate and Atmospheric Science*, 5(1), 32. Re-
696 trieved from <https://doi.org/10.1038/s41612-022-00254-6> doi:
697 10.1038/s41612-022-00254-6
- 698 Crutzen, P. J. (2006). Albedo enhancement by stratospheric sulfur injections: a
699 contribution to resolve a policy dilemma? [Journal Article]. *Climatic change*,
700 77(3-4), 211.
- 701 Dhomse, S. S., Mann, G. W., Antuña Marrero, J. C., Shallcross, S. E., Chipperfield,
702 M. P., Carslaw, K. S., ... Johnson, C. E. (2020). Evaluating the simulated
703 radiative forcings, aerosol properties, and stratospheric warmings from the
704 1963 mt Agung, 1982 el Chichón, and 1991 mt Pinatubo volcanic aerosol clouds
705 [Journal Article]. *Atmospheric Chemistry and Physics*, 20(21), 13627-13654.
- 706 Dykema, J. A., Keith, D. W., & Keutsch, F. N. (2016). Improved aerosol radiative
707 properties as a foundation for solar geoengineering risk assessment. *Geophysical
708 Research Letters*, 43(14), 7758-7766.
- 709 Fasullo, J. T., & Richter, J. H. (2022). Scenario and model dependence of strategic
710 solar climate intervention in CESM [Journal Article]. *EGU Sphere*, 2022, 1-30.
- 711 Frierson, D. M., Hwang, Y.-T., Fučkar, N. S., Seager, R., Kang, S. M., Donohoe, A.,
712 ... Battisti, D. S. (2013). Contribution of ocean overturning circulation to
713 tropical rainfall peak in the northern hemisphere. *Nature Geoscience*, 6(11),
714 940-944.
- 715 Haigh, J. D., Blackburn, M., & Day, R. (2005). The response of tropospheric
716 circulation to perturbations in lower-stratospheric temperature [Journal Ar-
717 ticle]. *Journal of Climate*, 18(17), 3672-3685. Retrieved from [https://
718 journals.ametsoc.org/view/journals/clim/18/17/jcli3472.1.xml](https://journals.ametsoc.org/view/journals/clim/18/17/jcli3472.1.xml) doi:
719 <https://doi.org/10.1175/JCLI3472.1>
- 720 Haywood, J., Tilmes, S., Jones, A., Keutsch, F., Laakso, A., Niemeier, U., ... Yu,
721 P. (2022). Stratospheric aerosol injection and its potential effect on the strato-
722 spheric ozone layer. In *Scientific assessment of ozone depletion: 2022* (pp.
723 325-383). World Meteorological Organization.
- 724 Haywood, J. M., Jones, A., Bellouin, N., & Stephenson, D. (2013). Asymmetric
725 forcing from stratospheric aerosols impacts Sahelian rainfall. *Nature Climate
726 Change*, 3(7), 660-665.
- 727 Haywood, J. M., Jones, A., Johnson, B. T., & McFarlane Smith, W. (2022). Assess-
728 ing the consequences of including aerosol absorption in potential stratospheric
729 aerosol injection climate intervention strategies. *Atmospheric Chemistry and
730 Physics*, 22(9), 6135-6150.
- 731 Held, I. M. (2000). *The general circulation of the atmosphere* [Conference Paper].
- 732 Henry, M., Haywood, J., Jones, A., Dalvi, M., Wells, A., Visioni, D., ... Tye, M.
733 (2023). Comparison of UKESM1 and CESM2 simulations using the same multi-
734 target stratospheric aerosol injection strategy [Journal Article]. *EGU Sphere*,
735 2023, 1-22.
- 736 Hueholt, D. M., Barnes, E. A., Hurrell, J. W., Richter, J. H., & Sun, L. (2023).
737 Assessing outcomes in stratospheric aerosol injection scenarios shortly after
738 deployment. *Earth's Future*, 11(5), e2023EF003488.
- 739 Iturbide, M., Gutiérrez, J. M., Alves, L. M., Bedia, J., Cerezo-Mota, R., Cimadevil-
740 lla, E., ... Gorodetskaya, I. V. (2020). An update of IPCC climate reference
741 regions for subcontinental analysis of climate model data: definition and ag-
742 gregated datasets [Journal Article]. *Earth System Science Data*, 12(4), 2959-
743 2970.
- 744 Jones, A., Haywood, J., Boucher, O., Kravitz, B., & Robock, A. (2010). Geoengi-
745 neering by stratospheric SO₂ injection: results from the Met Office HadGEM2

- 746 climate model and comparison with the goddard institute for space studies
747 modele [Journal Article]. *Atmospheric Chemistry and Physics*, 10(13), 5999-
748 6006.
- 749 Jones, A., Haywood, J. M., Jones, A. C., Tilmes, S., Kravitz, B., & Robock, A.
750 (2020). North atlantic oscillation response in geomip experiments g6solar
751 and g6sulfur: why detailed modelling is needed for understanding regional
752 implications of solar radiation management [Journal Article].
- 753 Jones, A. C., Haywood, J. M., Dunstone, N., Emanuel, K., Hawcroft, M. K., Hodges,
754 K. I., & Jones, A. (2017). Impacts of hemispheric solar geoengineering on
755 tropical cyclone frequency. *Nature Communications*, 8(1), 1382.
- 756 Jones, A. C., Haywood, J. M., Jones, A., & Aquila, V. (2016). Sensitivity of volcanic
757 aerosol dispersion to meteorological conditions: A pinatubo case study. *Journal*
758 *of Geophysical Research: Atmospheres*, 121(12), 6892–6908.
- 759 Kleidon, A., Kravitz, B., & Renner, M. (2015). The hydrological sensitivity to global
760 warming and solar geoengineering derived from thermodynamic constraints
761 [Journal Article]. *Geophysical Research Letters*, 42(1), 138-144. Retrieved
762 from [https://agupubs.onlinelibrary.wiley.com/doi/abs/10.1002/](https://agupubs.onlinelibrary.wiley.com/doi/abs/10.1002/2014GL062589)
763 [2014GL062589](https://doi.org/10.1002/2014GL062589) doi: <https://doi.org/10.1002/2014GL062589>
- 764 Kravitz, B., Caldeira, K., Boucher, O., Robock, A., Rasch, P. J., Alterskjaer, K.,
765 ... Haywood, J. M. (2013). Climate model response from the geoengineering
766 model intercomparison project (geomip) [Journal Article]. *Journal of Geophys-*
767 *ical Research: Atmospheres*, 118(15), 8320-8332.
- 768 Kravitz, B., MacMartin, D. G., Mills, M. J., Richter, J. H., Tilmes, S., Lamarque,
769 J., ... Vitt, F. (2017). First simulations of designing stratospheric sulfate
770 aerosol geoengineering to meet multiple simultaneous climate objectives [Jour-
771 nal Article]. *Journal of Geophysical Research: Atmospheres*, 122(23), 12,616-
772 12,634.
- 773 Kravitz, B., MacMartin, D. G., Tilmes, S., Richter, J. H., Mills, M. J., Cheng, W.,
774 ... Simpson, I. R. (2019). Comparing surface and stratospheric impacts of
775 geoengineering with different so2 injection strategies [Journal Article]. *Journal*
776 *of Geophysical Research: Atmospheres*, 124(14), 7900-7918.
- 777 Kravitz, B., MacMartin, D. G., Wang, H., & Rasch, P. J. (2016). Geoengineering as
778 a design problem [Journal Article]. *Earth System Dynamics*, 7(2), 469-497.
- 779 Kravitz, B., Robock, A., Tilmes, S., Boucher, O., English, J. M., Irvine, P. J.,
780 ... Watanabe, S. (2015). The geoengineering model intercomparison
781 project phase 6 (geomip6): simulation design and preliminary results [Jour-
782 nal Article]. *Geosci. Model Dev.*, 8(10), 3379-3392. Retrieved from
783 <https://gmd.copernicus.org/articles/8/3379/2015/> (GMD) doi:
784 [10.5194/gmd-8-3379-2015](https://doi.org/10.5194/gmd-8-3379-2015)
- 785 Laakso, A., Korhonen, H., Romakkaniemi, S., & Kokkola, H. (2017). Radiative and
786 climate effects of stratospheric sulfur geoengineering using seasonally varying
787 injection areas. *Atmospheric Chemistry and Physics*, 17(11), 6957–6974.
- 788 Lee, W. R., Vioni, D., Bednarz, E. M., MacMartin, D. G., Kravitz, B., & Tilmes,
789 S. (2023). Quantifying the efficiency of stratospheric aerosol geoengineer-
790 ing at different altitudes [Journal Article]. *Geophysical Research Letters*,
791 50(14), e2023GL104417. Retrieved from [https://agupubs.onlinelibrary](https://agupubs.onlinelibrary.wiley.com/doi/abs/10.1029/2023GL104417)
792 [.wiley.com/doi/abs/10.1029/2023GL104417](https://doi.org/10.1029/2023GL104417) doi: [https://doi.org/10.1029/](https://doi.org/10.1029/2023GL104417)
793 [2023GL104417](https://doi.org/10.1029/2023GL104417)
- 794 Lu, J., Vecchi, G. A., & Reichler, T. (2007). Expansion of the hadley cell under
795 global warming [Journal Article]. *Geophysical Research Letters*, 34(6).
- 796 Ma, J., Xie, S.-P., & Kosaka, Y. (2012). Mechanisms for tropical tropospheric circu-
797 lation change in response to global warming [Journal Article]. *Journal of Cli-*
798 *mate*, 25(8), 2979-2994.
- 799 MacMartin, D. G., & Kravitz, B. (2019). The engineering of climate engineering
800 [Journal Article]. *Annual Review of Control, Robotics, and Autonomous Sys-*

- 801 *tems*, 2(1), 445-467. Retrieved from [https://www.annualreviews.org/](https://www.annualreviews.org/doi/abs/10.1146/annurev-control-053018-023725)
 802 [doi/abs/10.1146/annurev-control-053018-023725](https://www.annualreviews.org/doi/abs/10.1146/annurev-control-053018-023725) doi: 10.1146/
 803 [annurev-control-053018-023725](https://www.annualreviews.org/doi/abs/10.1146/annurev-control-053018-023725)
- 804 MacMartin, D. G., Kravitz, B., Long, J. C. S., & Rasch, P. J. (2016). Geoengi-
 805 neering with stratospheric aerosols: What do we not know after a decade
 806 of research? [Journal Article]. *Earth's Future*, 4(11), 543-548. Retrieved
 807 from [https://agupubs.onlinelibrary.wiley.com/doi/abs/10.1002/](https://agupubs.onlinelibrary.wiley.com/doi/abs/10.1002/2016EF000418)
 808 [2016EF000418](https://agupubs.onlinelibrary.wiley.com/doi/abs/10.1002/2016EF000418) doi: <https://doi.org/10.1002/2016EF000418>
- 809 MacMartin, D. G., Kravitz, B., Tilmes, S., Richter, J. H., Mills, M. J., Lamarque,
 810 J.-F., ... Vitt, F. (2017). The climate response to stratospheric aerosol
 811 geoengineering can be tailored using multiple injection locations. *Journal of*
 812 *Geophysical Research: Atmospheres*, 122(23), 12–574.
- 813 MacMartin, D. G., Ricke, K. L., & Keith, D. W. (2018). Solar geoengineering as
 814 part of an overall strategy for meeting the 1.5 c paris target [Journal Article].
 815 *Philosophical Transactions of the Royal Society A: Mathematical, Physical and*
 816 *Engineering Sciences*, 376(2119), 20160454.
- 817 MacMartin, D. G., Visioni, D., Kravitz, B., Richter, J., Felgenhauer, T., Lee, W.,
 818 ... Sugiyama, M. (2022). Scenarios for modeling solar radiation modification.
 819 *Proceedings of the National Academy of Sciences*, 119(33), e2202230119.
- 820 Mann, G., Carslaw, K., Spracklen, D., Ridley, D., Manktelow, P., Chipperfield, M.,
 821 ... Johnson, C. (2010). Description and evaluation of glomap-mode: A modal
 822 global aerosol microphysics model for the ukca composition-climate model
 823 [Journal Article]. *Geoscientific Model Development*, 3(2), 519-551.
- 824 Masson-Delmotte, V., Zhai, P., Pirani, S., Connors, C., Péan, S., Berger, N., ...
 825 Scheel Monteiro, P. M. (2021). Ipcc, 2021: Summary for policymakers. in: Cli-
 826 mate change 2021: The physical science basis. contribution of working group
 827 i to the sixth assessment report of the intergovernmental panel on climate
 828 change.
- 829 Maycock, A. C., Joshi, M. M., Shine, K. P., & Scaife, A. A. (2013). The circulation
 830 response to idealized changes in stratospheric water vapor [Journal Article].
 831 *Journal of Climate*, 26(2), 545-561.
- 832 Niemeier, U., & Schmidt, H. (2017). Changing transport processes in the strato-
 833 sphere by radiative heating of sulfate aerosols [Journal Article]. *Atmospheric*
 834 *Chemistry and Physics*, 17(24), 14871-14886.
- 835 Niemeier, U., Schmidt, H., Alterskjær, K., & Kristjánsson, J. E. (2013). Solar
 836 irradiance reduction via climate engineering: Impact of different techniques
 837 on the energy balance and the hydrological cycle [Journal Article]. *Journal*
 838 *of Geophysical Research: Atmospheres*, 118(21), 11,905-11,917. Retrieved
 839 from [https://agupubs.onlinelibrary.wiley.com/doi/abs/10.1002/](https://agupubs.onlinelibrary.wiley.com/doi/abs/10.1002/2013JD020445)
 840 [2013JD020445](https://agupubs.onlinelibrary.wiley.com/doi/abs/10.1002/2013JD020445) doi: <https://doi.org/10.1002/2013JD020445>
- 841 Niemeier, U., Schmidt, H., & Timmreck, C. (2011). The dependency of geoengi-
 842 neered sulfate aerosol on the emission strategy [Journal Article]. *Atmospheric*
 843 *Science Letters*, 12(2), 189-194.
- 844 O'Neill, B. C., Tebaldi, C., Van Vuuren, D. P., Eyring, V., Friedlingstein, P., Hurtt,
 845 G., ... Lowe, J. (2016). The scenario model intercomparison project (scenar-
 846 iomip) for cmip6 [Journal Article]. *Geoscientific Model Development*, 9(9),
 847 3461-3482.
- 848 Pan, R., Shu, Q., Wang, Q., Wang, S., Song, Z., He, Y., & Qiao, F. (2023). Future
 849 arctic climate change in cmip6 strikingly intensified by nemo-family climate
 850 models. *Geophysical Research Letters*, 50(4), e2022GL102077.
- 851 Programme, U. N. E. (2021). *Emissions gap report 2021: The heat is on - a world of*
 852 *climate promised not yet delivered*. [Book]. UN.
- 853 Punge, H., Konopka, P., Giorgetta, M., & Müller, R. (2009). Effects of the quasi-
 854 biennial oscillation on low-latitude transport in the stratosphere derived from
 855 trajectory calculations [Journal Article]. *Journal of Geophysical Research:*

- 856 *Atmospheres*, 114(D3).
- 857 Rasch, P. J., Tilmes, S., Turco, R. P., Robock, A., Oman, L., Chen, C.-C., ... Gar-
858 cia, R. R. (2008). An overview of geoengineering of climate using stratospheric
859 sulphate aerosols [Journal Article]. *Philosophical Transactions of the Royal*
860 *Society A: Mathematical, Physical and Engineering Sciences*, 366(1882), 4007-
861 4037. Retrieved from [https://royalsocietypublishing.org/doi/abs/](https://royalsocietypublishing.org/doi/abs/10.1098/rsta.2008.0131)
862 [10.1098/rsta.2008.0131](https://royalsocietypublishing.org/doi/abs/10.1098/rsta.2008.0131) ((Jack)) doi: doi:10.1098/rsta.2008.0131
- 863 Richter, J., Vioni, D., MacMartin, D., Bailey, D., Rosenbloom, N., Lee, W., ...
864 Lamarque, J.-F. (2022). Assessing responses and impacts of solar climate
865 intervention on the earth system with stratospheric aerosol injection (arise-sai)
866 [Journal Article]. *EGUsphere*, 1-35.
- 867 Ricke, K., Wan, J. S., Saenger, M., & Lutsko, N. J. (2023). Hydrological conse-
868 quences of solar geoengineering [Journal Article]. *Annual Review of Earth and*
869 *Planetary Sciences*, 51, 447-470.
- 870 Ridley, J. K., Blockley, E. W., Keen, A. B., Rae, J. G. L., West, A. E., & Schroeder,
871 D. (2018). The sea ice model component of hadgem3-gc3.1 [Journal Ar-
872 ticle]. *Geoscientific Model Development*, 11(2), 713-723. doi: 10.5194/
873 gmd-11-713-2018
- 874 Robock, A., MacMartin, D. G., Duren, R., & Christensen, M. W. (2013). Studying
875 geoengineering with natural and anthropogenic analogs [Journal Article]. *Cli-*
876 *matic Change*, 121(3), 445-458. Retrieved from [https://doi.org/10.1007/](https://doi.org/10.1007/s10584-013-0777-5)
877 [s10584-013-0777-5](https://doi.org/10.1007/s10584-013-0777-5) doi: 10.1007/s10584-013-0777-5
- 878 Schneider, T., O’Gorman, P. A., & Levine, X. J. (2010). Water vapor and the dy-
879 namics of climate changes [Journal Article]. *Reviews of Geophysics*, 48(3).
880 Retrieved from [https://agupubs.onlinelibrary.wiley.com/doi/abs/](https://agupubs.onlinelibrary.wiley.com/doi/abs/10.1029/2009RG000302)
881 [10.1029/2009RG000302](https://agupubs.onlinelibrary.wiley.com/doi/abs/10.1029/2009RG000302) doi: <https://doi.org/10.1029/2009RG000302>
- 882 Sellar, A. A., Jones, C. G., Mulcahy, J. P., Tang, Y., Yool, A., Wiltshire, A., ...
883 Zerroukat, M. (2019). Ukesm1: Description and evaluation of the u.k. earth
884 system model [Journal Article]. *Journal of Advances in Modeling Earth Sys-*
885 *tems*, 11(12), 4513-4558. doi: 10.1029/2019ms001739
- 886 Seneviratne, S. I., Zhang, X., Adnan, M., Badi, W., Dereczynski, C., Di Luca, A.,
887 ... Zhou, B. (2021). 11 chapter 11: Weather and climate extreme events in a
888 changing climate [Journal Article].
- 889 Seo, K., Frierson, D. M., & Son, J. (2014). A mechanism for future changes in
890 hadley circulation strength in cmip5 climate change simulations [Journal Arti-
891 cle]. *Geophysical Research Letters*, 41(14), 5251-5258.
- 892 Simpson, I., Tilmes, S., Richter, J., Kravitz, B., MacMartin, D., Mills, M. J., ...
893 Pendergrass, A. G. (2019). The regional hydroclimate response to stratospheric
894 sulfate geoengineering and the role of stratospheric heating [Journal Article].
895 *Journal of Geophysical Research: Atmospheres*, 124(23), 12587-12616.
- 896 Staten, P. W., Lu, J., Grise, K. M., Davis, S. M., & Birner, T. (2018). Re-examining
897 tropical expansion [Journal Article]. *Nature Climate Change*, 8(9), 768-
898 775. Retrieved from <https://doi.org/10.1038/s41558-018-0246-2> doi:
899 [10.1038/s41558-018-0246-2](https://doi.org/10.1038/s41558-018-0246-2)
- 900 Storkey, D., Blaker, A. T., Mathiot, P., Megann, A., Aksenov, Y., Blockley, E. W.,
901 ... Sinha, B. (2018). Uk global ocean go6 and go7: a traceable hierarchy of
902 model resolutions [Journal Article]. *Geoscientific Model Development*, 11(8),
903 3187-3213. doi: 10.5194/gmd-11-3187-2018
- 904 Swaminathan, R., Parker, R. J., Jones, C. G., Allan, R. P., Quaife, T., Kelley, D. I.,
905 ... Walton, J. (2022). The physical climate at global warming thresholds
906 as seen in the uk earth system model [Journal Article]. *Journal of Climate*,
907 35(1), 29-48.
- 908 Tilmes, S., Fasullo, J., Lamarque, J., Marsh, D. R., Mills, M., Alterskjaer, K., ...
909 Schulz, M. (2013). The hydrological impact of geoengineering in the geoengi-
910 neering model intercomparison project (geomip) [Journal Article]. *Journal of*

- 911 *Geophysical Research: Atmospheres*, 118(19), 11,036-11,058.
- 912 Tilmes, S., Richter, J. H., Kravitz, B., MacMartin, D. G., Glanville, A. S., Vi-
913 sioni, D., ... Müller, R. (2021). Sensitivity of total column ozone to
914 stratospheric sulfur injection strategies [Journal Article]. *Geophysical*
915 *Research Letters*, 48(19), e2021GL094058. Retrieved from [https://](https://agupubs.onlinelibrary.wiley.com/doi/abs/10.1029/2021GL094058)
916 agupubs.onlinelibrary.wiley.com/doi/abs/10.1029/2021GL094058 doi:
917 <https://doi.org/10.1029/2021GL094058>
- 918 Tilmes, S., Richter, J. H., Kravitz, B., MacMartin, D. G., Mills, M. J., Simpson,
919 I. R., ... Lamarque, J.-F. (2018). Cesm1 (waccm) stratospheric aerosol geo-
920 engineering large ensemble project [Journal Article]. *Bulletin of the American*
921 *Meteorological Society*, 99(11), 2361-2371.
- 922 Tilmes, S., Richter, J. H., Mills, M. J., Kravitz, B., MacMartin, D. G., Garcia,
923 R. R., ... Vitt, F. (2018). Effects of different stratospheric so2 injection
924 altitudes on stratospheric chemistry and dynamics [Journal Article]. *Jour-*
925 *nal of Geophysical Research: Atmospheres*, 123(9), 4654-4673. Retrieved
926 from [https://](https://agupubs.onlinelibrary.wiley.com/doi/abs/10.1002/2017JD028146)
927 [agupubs.onlinelibrary.wiley.com/doi/abs/10.1002/](https://agupubs.onlinelibrary.wiley.com/doi/abs/10.1002/2017JD028146)
928 [2017JD028146](https://agupubs.onlinelibrary.wiley.com/doi/abs/10.1002/2017JD028146) doi: <https://doi.org/10.1002/2017JD028146>
- 928 Tilmes, S., Visioni, D., Jones, A., Haywood, J., Séférian, R., Nabat, P., ... Niemeier,
929 U. (2022). Stratospheric ozone response to sulfate aerosol and solar dimming
930 climate interventions based on the g6 geoengineering model intercomparison
931 project (geomip) simulations [Journal Article].
- 932 Trenberth, K. E., & Dai, A. (2007). Effects of mount pinatubo volcanic eruption
933 on the hydrological cycle as an analog of geoengineering [Journal Article]. *Geo-*
934 *physical Research Letters*, 34(15).
- 935 UNEP, U. N. E. P. (2023). *One atmosphere: An independent expert review on so-*
936 *lar radiation modification research and deployment*. Retrieved from [https://](https://wedocs.unep.org/20.500.11822/41903)
937 wedocs.unep.org/20.500.11822/41903
- 938 Vallis, G. K., Zurita-Gotor, P., Cairns, C., & Kidston, J. (2015). Response of the
939 large-scale structure of the atmosphere to global warming [Journal Article].
940 *Quarterly Journal of the Royal Meteorological Society*, 141(690), 1479-1501.
- 941 Visioni, D., Bednarz, E. M., Lee, W. R., Kravitz, B., Jones, A., Haywood, J. M., &
942 MacMartin, D. G. (2023). Climate response to off-equatorial stratospheric
943 sulfur injections in three earth system models—part 1: Experimental protocols
944 and surface changes. *Atmospheric Chemistry and Physics*, 23(1), 663–685.
- 945 Visioni, D., MacMartin, D. G., Kravitz, B., Bednarz, E. M., & Goddard, P. B.
946 (2023). The choice of baseline period influences the assessments of the out-
947 comes of stratospheric aerosol injection. *Authorea Preprints*.
- 948 Visioni, D., MacMartin, D. G., Kravitz, B., Boucher, O., Jones, A., Lurton, T.,
949 ... Niemeier, U. (2021). Identifying the sources of uncertainty in climate
950 model simulations of solar radiation modification with the g6sulfur and g6solar
951 geoengineering model intercomparison project (geomip) simulations [Journal
952 Article]. *Atmospheric Chemistry and Physics*, 21(13), 10039-10063.
- 953 Visioni, D., MacMartin, D. G., Kravitz, B., Lee, W., Simpson, I. R., & Richter,
954 J. H. (2020). Reduced poleward transport due to stratospheric heating under
955 stratospheric aerosols geoengineering. *Geophysical Research Letters*, 47(17),
956 e2020GL089470.
- 957 Visioni, D., Pitari, G., Tuccella, P., & Curci, G. (2018). Sulfur deposition
958 changes under sulfate geoengineering conditions: quasi-biennial oscilla-
959 tion effects on the transport and lifetime of stratospheric aerosols [Jour-
960 nal Article]. *Atmos. Chem. Phys.*, 18(4), 2787-2808. Retrieved from
961 <https://acp.copernicus.org/articles/18/2787/2018/> (ACP) doi:
962 [10.5194/acp-18-2787-2018](https://doi.org/10.5194/acp-18-2787-2018)
- 963 Waugh, D. W., Grise, K. M., Seviour, W. J., Davis, S. M., Davis, N., Adam, O., ...
964 Maycock, A. C. (2018). Revisiting the relationship among metrics of tropical
965 expansion [Journal Article]. *Journal of Climate*, 31(18), 7565-7581.

- 966 Wells, A. F., Henry, M., & Bednarz, E. M. (2023). *Code for "identifying climate im-*
967 *acts from different stratospheric aerosol injection strategies in ukesm1"* [code].
968 Zenodo. Retrieved from <https://doi.org/10.5281/zenodo.10302916> doi:
969 10.5281/zenodo.10302916
- 970 Wells, A. F., Jones, A., & Dalvi, M. (2023). *Data for "identifying climate impacts*
971 *from different stratospheric aerosol injection strategies in ukesm1"* [dataset].
972 Zenodo. Retrieved from <https://doi.org/10.5281/zenodo.10302574> doi:
973 10.5281/zenodo.10302574
- 974 Wells, A. F., Jones, A., Osborne, M., Damany-Pearce, L., Partridge, D. G., & Hay-
975 wood, J. M. (2023). Including ash in ukesm1 model simulations of the raikoke
976 volcanic eruption reveals improved agreement with observations [Journal Arti-
977 cle]. *Atmospheric Chemistry and Physics*, *23*(7), 3985-4007.
- 978 Wheeler, T., & Von Braun, J. (2013). Climate change impacts on global food secu-
979 rity [Journal Article]. *Science*, *341*(6145), 508-513.
- 980 Yool, A., Popova, E. E., & Anderson, T. R. (2013). Medusa-2.0: an intermedi-
981 ate complexity biogeochemical model of the marine carbon cycle for climate
982 change and ocean acidification studies [Journal Article]. *Geoscientific Model*
983 *Development*, *6*(5), 1767-1811. doi: 10.5194/gmd-6-1767-2013
- 984 Zhang, Y., MacMartin, D. G., Visioni, D., Bednarz, E., & Kravitz, B. (2023). Intro-
985 ducing a comprehensive set of stratospheric aerosol injection strategies. *EGU-*
986 *sphere*, *2023*, 1–32.
- 987 Zhao, M., Cao, L., Bala, G., & Duan, L. (2021). Climate response to latitudinal and
988 altitudinal distribution of stratospheric sulfate aerosols. *Journal of Geophysical*
989 *Research: Atmospheres*, *126*(24), e2021JD035379. Retrieved from [https://](https://agupubs.onlinelibrary.wiley.com/doi/abs/10.1029/2021JD035379)
990 agupubs.onlinelibrary.wiley.com/doi/abs/10.1029/2021JD035379
991 (e2021JD035379 2021JD035379) doi: <https://doi.org/10.1029/2021JD035379>